THE ASYMMETRIC BACK EXOSUIT: DESIGN, REALIZATION AND BIOMECHANICAL EVALUATION

A Dissertation
Presented to
The Academic Faculty

by

Jared Michael Li

In Partial Fulfillment
of the Requirements for the Degree
Master of Science in Mechanical Engineering in the
Woodruff School of Mechanical Engineering

Georgia Institute of Technology
December 2020

THE ASYMMETRIC BACK EXOSUIT: DESIGN, REALIZATION AND BIOMECHANICAL EVALUATION

Approved by:

Dr. Aaron Young, Advisor
School of Mechanical Engineering
Georgia Institute of Technology

Dr. Anirban Mazumdar
School of Mechanical Engineering
Georgia Institute of Technology

Dr. Gregory Sawicki
School of Mechanical Engineering
Georgia Institute of Technology

Date Approved: December 01, 2020

To the past, present, and future members of EPIC Lab.

ACKNOWLEDGEMENTS

First, I would like to thank my reading committee for guiding me through this process and being invaluable sources of ideas and inspiration. Secondly, I want to thank the PhD students of EPIC Lab for being my dear friends and providing me with perspective when issues arise. Krishan Bhakta and Jonathan Camargo have my sincere gratitude for introducing me to prosthetics and exoskeleton research as well as being incredible mentors throughout my undergraduate degree. I would also like to thank Dean Molinaro for being my invaluable research partner and mentor in my master's without whom I would not be where I am today.

Third, I want to thank Dr. Aaron Young for being my advisor throughout undergraduate and graduate school. Under Dr. Young's care, I have greatly expanded my skillset, obtained a greater understanding of biomedical, electrical, and mechanical engineering, and have developed an appreciation for the work it takes to properly conduct scientific research. Fourth, I thank the FAB-X senior capstone team for an amazing end to the undergraduate degree and for putting me in a position to succeed. Fifth, many thanks to my outstanding team of undergraduate students, specifically Andrew King, Allen Zhang, Chris Ray, Paul Matesevac, Courtney Wolpov, James McCormick, Jordyn Sak, Keturah Mort, and Pedro Vieira. Lastly, I would like to extend my love and thanks to my parents, grandparents, extended family, friends, and my girlfriend Elizabeth for their unwavering support in my academic pursuits.

TABLE OF CONTENTS

LIST OF TABLES

LIST OF FIGURES

LIST OF SYMBOLS AND ABBREVIATIONS

ABX	Asymmetric Back Exosuit
LBP	Low Back Pain
MMH	Manual Materials Handling
EMG	Electromyography
IMU	Inertial Measurement Unit
DoF	Degree of Freedom
s_m	Exosuit Cable Tension
τ_t	Induced Lumbar Torque
$\dot{l}_m$	Cable Shortening Speed
r_θ	Generalized Effective Moment Arm
ω_θ	Generalized Biological Joint Velocity
τ_{motor}	Motor Torque
ω_{motor}	Motor Angular Velocity
d_{pulley}	Pulley Major Diameter
R	Speed Reduction / Torque Amplification
N_x	Gear Tooth Number
CNC	Computer Numerical Control
EDM	Electrical Discharge Machining
MC	Microcontroller
ESC	Electronic Speed Controller
FSM	Finite State Machine
s_d	Desired Cable Tension

ω_{cmd}	Commanded Motor Velocity
s	Measured Cable Tension
ω_t	Trunk Extension Velocity
k_s	Cable Tension Control Gain
k_h	Trunk Velocity Control Gain
θ_t	Trunk Extension Angle
θ_0	Stand Angle
θ_b	Bent Angle
ω_{FA}	Full Assistance Velocity Threshold
ω_{OFF}	Transparency Mode Transition Velocity
n	Subject Count
RoM	Range of Motion
SYM	Symmetric
ASYM90	Asymmetric 90°
ASYM180	Asymmetric 180°
LLES	Left Lumbar Erector Spinae
RLES	Right Lumbar Erector Spinae
LLD	Left Latissimus Dorsi
RLD	Right Latissimus Dorsi
LEO	Left External Oblique
REO	Right External Oblique
RA	Rectus Abdominis
rEMG	Root Mean Squared EMG
SEM	Standard Error of the Mean

a	Musculotendon Actuator
τ_θ	Torque Induced at a Biological DoF
s_a	Tension Force of a Musculotendon Actuator
q	Generalized Coordinates of Musculoskeletal Model
l	Path of a Musculotendon Actuator
$f(s)$	Generalized Force Matrix of Musculoskeletal Model
C_θ	Joint-Specific Geometric Coupling Matrix
s_0	Unit Tension
W_θ	Assistive Torque Workspace of a DoF
R_θ	Effective Cable Moment Arm Vector
$S_{MIN/MAX}$	Minimum / Maximum Cable Tension
J_θ	Maximum Restorative Torque of the ABX
iEMG	Integrated EMG
pEMG	Peak EMG
BW	Bodyweight

SUMMARY

Musculoskeletal disorders of the back are an extremely prevalent health issue across the workforce in the United States. This is especially a concern in industries involving manual materials handling tasks that cause low back pain. While these injuries are generated by both symmetric and asymmetric lifting, asymmetric movements are often more damaging. Exoskeleton technology has become an increasingly popular preventative measure to low back pain, but many devices do not assist in asymmetry. Thus, I present a new system called the Asymmetric Back Exosuit (ABX). The ABX addresses this important gap in the field through unique design geometry and active cable-driven actuation. The suit allows the user to move in a wide range of lumbar trajectories while the "X" pattern cable routing allows for variable assistance application for these trajectories, enabling assistance during asymmetric movements. As indicated by a biomechanical model of the system made in OpenSim, the cable forces can be mapped to effective lumbar torque assistance for a given lumbar trajectory, allowing for intuitive controller design over the complex kinematic chain for varying lifting techniques. An early human subject study indicated that the ABX was able to reduce low back muscle activation during symmetric and asymmetric lifting by an average of 37.8% and 16.0%, respectively, compared to lifting without the exosuit. This was expanded to a larger biomechanics study of the ABX for which preliminary results of three subjects are examined and discussed. These evaluations indicate the potential for the ABX to reduce lumbar injury risk during symmetric and asymmetric manual materials handling tasks.

CHAPTER 1. INTRODUCTION

1.1 Low Back Pain

Often described as one of the most prevalent health issues in the United States and abroad, Low back pain (LBP) causes physical pain, reduction to quality of life, and economic hardship [1]–[3]. For example, it has been estimated that LBP causes approximately $20 billion a year in direct medical costs, and $100 to $200 billion annually when considering indirect costs, such as lost wages due to work absence [4]. However, the prevalence of LBP continues to rise despite these adverse consequences. For instance, Freburger *et al.* surveyed North Carolina households in 1992 and 2006 finding that LBP prevalence doubled over the 14-year timeframe [5]. Further, the United States Bureau of Labor Statistics reported that 38.5% of all work-related musculoskeletal disorders involved the back in 2016, indicating the persistence of LBP in both the general population and industry [6].

1.1.1 Causes of Injury

Common among industries in which there is high risk for LBP is the presence of manual materials handling (MMH) tasks [7]. As such, MMH tasks, such as lifting objects with high frequency and intensity, have been found to be a predictors of LBP in several previous studies [8]–[10]. Biomechanically, the lumbar spine and lumbar muscles are usually indicated as the most affected areas [11]. During lifting, trunk extensor muscles, primarily the erector spinae groups, generate extension moments along the trunk to stabilize the spine [12], [13]. Frequent and high-load MMH activities repeatedly require

the generation of these biological moments which increases the risk for strain in the erector spinae muscles, prolapse or protrusion of intervertebral discs from compression and shear in the lumbar spine, and damage to the vertebral column, all of which can induce LBP [12], [14]. Though symmetric restricted to the sagittal plane can inflict this damage, asymmetric lifting involving twisting the lumbar spine can exacerbate existing symptoms and increase the risk of LBP development [12], [15], [16]. Specifically, torso twist during lifting has been shown to reduce available trunk strength by up to 21% [17] and increase compressive and shear loading in the lumbosacral (L5/S1) joint during various MMH tasks [18] [19] [20] [21]. Although the additional danger of asymmetric lifting is apparent, it is present in many MMH-centered occupations [22]. Wearable supports, such as lifting belts and back braces, have been previously implemented and studied in industrial settings to combat LBP incidence rate but have shown little to no positive effect in reducing risk factors for LBP [23] [24] [25].

1.2 Exoskeleton and Exosuit Prior Art

Because of the lack of effective preventative measures for LBP, industrial exoskeleton technology has gained substantial interest. As a result, previous research has studied the benefit of applying external mechanical power to the user during lifting through two main categories of assistive devices: passive exosuits and active exoskeletons [26], [27]. Measuring muscle activation through electromyography (EMG) is a common way to quantify the performance of these devices [26]. This is due to low back muscle activation being tied to development of LBP as well as EMG being approximately related to extensor moment generation [12] [28].

1.2.1 Passive Exosuits

Passive exosuits generally use pliable materials and elastic elements to provide passive assistance during lifting [29]–[32]. The design philosophy of these systems has yielded devices that are lightweight and allow the user to maintain their natural range of motion. Additionally, assistive force is often applied parallel to the human vertebral column, comparable to back extensor muscle action, which mitigates adverse effects of actuator-joint misalignment [33]. These benefits make passive exosuits more suited for asymmetric lifting tasks [31], [34]. For example, the personal lift assistive device (PLAD) from Abdoli *et al.* was shown to be effective in reducing estimated moments in the lumbar spine, specifically the L4/L5 joint, by 14-20% and activation of the erector spinae by 14.4-27.6% in symmetric lifting of various loads [29]. This design was also studied in asymmetric lifting at a 45° angle between the sagittal and coronal planes showing that erector spinae activation was reduced by 21-31% and estimated lumbar moments were reduced by 24.5% about all 3 axes of rotation [34]. While unpowered, passive devices are able to positively affect human biomechanics while keeping overall weight and device obtrusiveness low.

However, these benefits come at the cost of fixed assistance dynamics based on the mechanical properties of the elastic elements used in the suits [33]. This prevents passive devices from being adaptable to changes in lifting conditions, such as variation in object weight, which is known to change the demands on biological joints [18], [21], [35]. Also, extreme dynamic lifting (e.g. lifting an object with a 180° trunk twist) has not previously been explored [31], [34].

1.2.2 Active Exoskeletons

Conversely, active back exoskeletons utilize rigid frames, powered actuators, and various sensing systems to deliver controllable mechanical power to the user during MMH tasks [36]–[40]. Common among these designs is high magnitude torque assistance applied at the hips, resulting in a significant decrease of EMG activation of the low back muscles. For example, Toxiri *et al.* evaluated an active back-support exoskeleton with torque capability of 40 Nm at the hip joint and assistance control through inertial measurement unit (IMU), proportional myoelectric control, and a hybrid mode that combines both [36]. In symmetric lifting of 7.5kg and 15kg, significant peak reductions in EMG of the left and right iliocostalis (erector spinae group) of 28-35% were observed across the control methods.

Though the assistance trajectory and magnitude can be effectively modulated for changes in task or user needs, these devices present significant drawbacks. For example, the increased weight from powered actuators and large batteries can be cumbersome, and rigid skeletal structures can restrict user range of motion [33]. Additionally, the actuators of active back exoskeletons are typically placed in-line with the user's joints, which can lead to parasitic forces that compromise device comfort and assistance controllability if misaligned [33], [41]. Further, the reduction in user range of motion and in-line actuator placement prevents most active back exoskeletons from assisting outside of the sagittal plane, limiting their benefits to symmetric lifting. Though asymmetry has been previously explored in active devices, no biological outcomes were measured [42], and extreme asymmetric movements were not evaluated [38].

1.2.3 Cable-Driven Actuation

Another method of applying active assistance is through the use of cable-driven actuation. This technique hybridizes the assistance techniques of passive and active systems since cables function similarly to parallel actuation methods (i.e. elastic elements) [43], [44]. Furthermore, induced moments can be modulated and amplified as needed by powered actuators [43], [44]. This method also allows for greater control authority over complex joint spaces with numerous DoFs [45], [46]. A good example of this implementation is the spine-inspired back exoskeleton from Yang *et al.* [47]. This device leverages a soft design mimicking a human spine interwoven with a Bowden cable actuated by an off-board motor-gear-pulley transmission capable of high linear force (up to 1500 N). Despite the advantages of cable-driven actuation, very little research has investigated the effects of cable-driven back assistive devices beyond limited symmetric motion [47], [48].

1.3 Novel Solution

Neither active nor passive devices have completely addressed the issue of assisting in asymmetric dynamic lifting. Specifically, there is a gap in the field for a device that exhibits key design requirements: (1) maintain user freedom of movement, (2) provide active lumbar torque assistance regardless of biological kinematics, (3) reduce low back muscle activation with active assistance. Responding to this gap, I, with teams of graduate and undergraduate students, designed, developed, and evaluated the ABX (Figure 1), a novel exosuit that combines a flexible, biologically-inspired structure common in passive

exosuits with controllable powered assistance application characteristic of active exoskeletons.

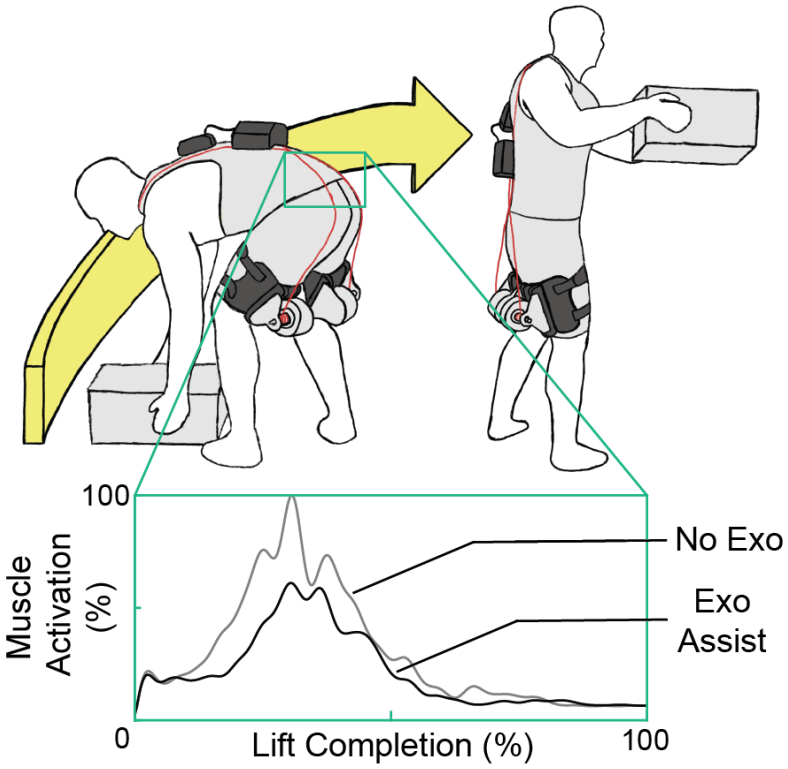

Figure 1 - The Asymmetric Back Exosuit (ABX) was designed to assist users during symmetric and asymmetric (shown here) lifting. ABX successfully reduced user lumbar erector spinae muscle activation during lifting compared to lifting without the exosuit.

By implementing a cable-driven approach, the suit is able to apply assistive force in symmetric and extreme asymmetric lifting, preserve users' range of motion, and provide assistive torque over the 3 axes of the L5/S1 joint while keeping the overall device lightweight and unobtrusive. Because of the novel design geometry of this device, I

hypothesize that, through human subject evaluation, the ABX is able to reduce risk factors for LBP in symmetric and asymmetric lifting.

1.4 Introduction to the Remainder of the Thesis

The remainder of this thesis details the design and development of the ABX as well as human subject biomechanical evaluation. Specifically, Chapter 2 explains the design rationale and mechanical and controls design and development. Chapter 3 details the methods and results of actuator validation, methods and results from the human-exosuit outcomes study, and the early EMG outcomes results from the biomechanics study. Finally, a discussion of the analyses and results from each study and final remarks are provided in Chapter 4.

CHAPTER 2. EXOSUIT DESIGN

2.1 Actuator Design

2.1.1 Rationale

We designed ABX using cable-driven actuation (Figure 2-A), which mimics the musculoskeletal system [44]. Cable-driven actuation provides three key benefits over actuators mounted in-line with biological joints for lumbar assistive devices: 1) cable-driven actuation can provide assistance over multiple degrees of freedom (DoFs) (i.e., the intervertebral and hip joints) without adding additional actuators or device joints [46], [47], [49]; 2) unlike rigid, in-line actuation interfaces, cable-driven systems maintain the decoupling of the assisted biological joints with minimal device complexity and weight [47]; and 3) with sufficient cable routing, the device actuators can be placed independently of biological joint location [47], [49]–[51], resulting in increased user comfort and offloading of the actuator weight from the lumbar. Given these benefits, cable-driven actuation allows the ABX to provide active assistance across the hip and intervertebral DoFs while preserving the user's range of motion. Further, we implemented two independently actuated cables that attach to each of the user's thighs and opposite shoulders, resulting in an "X" pattern crossing along the lumbar spine. This actuation geometry allows for the total assistance magnitude and relative assistance asymmetry to be independently controlled by the device.

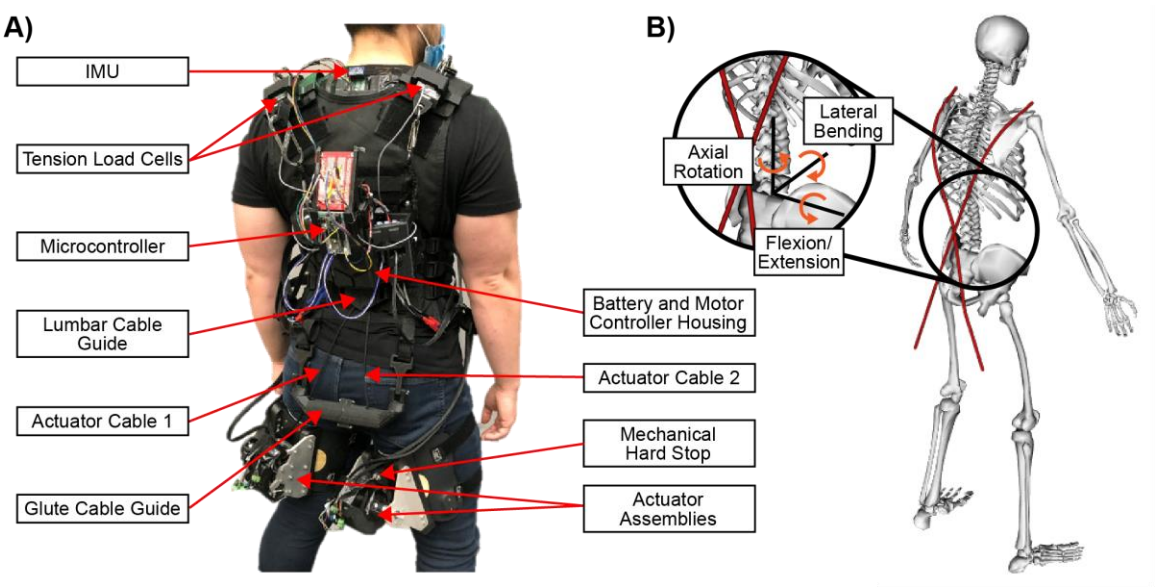

Figure 2 - A) The Asymmetric Back Exosuit (ABX) designed and validated in this study is shown. Thigh-mounted actuators tension the nylon cables attached to opposite shoulders to assist the user during symmetric and asymmetric lifting. Additionally, the microcontroller, batteries, and motor controllers are mounted on the back of the user, making the ABX a fully autonomous system. B) To characterize the mechanical advantage of the ABX on the lumbar spine, the actuator cables were modeled with respect to the user in OpenSim. As shown, the actuator cables generate an assistive torque in the flexion/extension, axial rotation, and lateral bending degrees of freedom of the lumbosacral joint located at the origin of the lumbar reference frame.

Despite these advantages, cable-driven actuation can result in a reduced mechanical advantage with respect to the lumbosacral joint compared to in-line actuation [36]–[40]. Thus, it was important to design the ABX actuators to generate sufficient cable force to provide active assistance benefits. Using a simplified two DoF (hip and lumbar extension) lifting model (Figure 3) similar to previous studies [52], [53], we designed our actuators such that the maximum induced lumbosacral extension assistance was larger than 100 Nm, which is approximately 50% of the peak biological moment in un-loaded trunk extension [54]. Some assumptions are made when using this model. First, the torque in the L5/S1 generated by flexion/extension is much greater than that induced by axial rotation or lateral

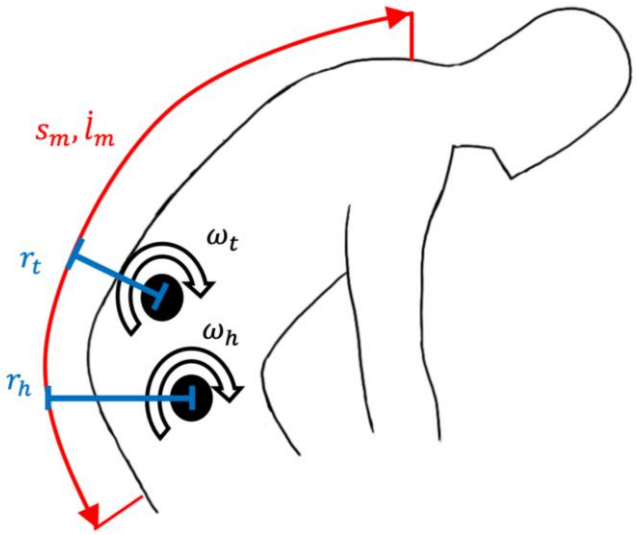

Figure 3 - Simplified 2-DoF model of the ABX cable action over the lumbosacral (L5/S1) and hip joints.

bending. Second, cable speed in flexion/extension is much greater than that in axial rotation or lateral bending. Third, perfect energy transfer occurs in the system (no losses to friction). Fourth, the kinematics of the lumbar spine are resolved to the kinematics of the L5/S1.

We computed a required tension in each cable (s_m) of 556 N to achieve a lumbar assistive torque (τ_t) of 100 Nm using a moment arm (r_t) of 9 cm [30] as

$$s_m = \frac{\tau_t}{2r_t}. \tag{1}$$

Additionally, we computed the maximum expected shortening speed of the cable $(\dot{l}_m)$ to ensure our actuators were not speed limited. Assuming lossless energy transfer between the cable and joint (θ), the effective moment arm (r_θ) can be expressed using the joint velocity (ω_θ) as

$$r_\theta = \frac{\dot{l}_m}{\omega_\theta}. \tag{2}$$

Thus, the maximum expected cable shortening speed was computed as 28.7 cm/s using normative hip and lumbar extension velocity trajectories during symmetric lifting [55], assuming constant moment arms of 9 cm for both the hip (r_h) and lumbosacral (r_t) joints using

$$\dot{l}_m = \max \sum_{i}^{n_\theta} r_i \omega_i \,. \tag{3}$$

2.1.2 Pulley and Speed Reduction Specification

Using these linear force and speed requirements, we designed and manufactured an actuator assembly for each cable of the exosuit. Driving each assembly is a U8-Lite KV100 brushless DC motor (T-Motor, Nanchang, Jiangxi, China), rated to provide a torque (τ_{motor}) of 2.42 Nm at 395.5 rad/s (ω_{motor}) (3777 rpm), which was further characterized by Lee *et al.* across several operating conditions [56]. Using a pulley major diameter (d_{pulley}) and a speed reduction/torque amplification (R) gives the following speed condition for selecting pulley diameter and speed reduction:

$$\left(\frac{\omega_{motor}}{\frac{d_{pulley}}{2}} \right) * \left(\frac{1}{R} \right) > \dot{l}_m \,. \tag{4}$$

Further, to satisfy the set force condition we use

$$\left(\frac{\tau_{motor}}{\frac{d_{pulley}}{2}}\right) * R > s_m \,. \tag{5}$$

Since the speed condition is the lower bound, the torque specification can be increased to allow for a greater range of assistance. To meet the above conditions, a pulley major diameter of 2.09 cm (0.83 in) and a speed reduction of 6 was chosen. The pulley diameter was selected to maximize force output of the actuator while maintaining a sufficient bend radius for the nylon actuation cable [57]. The actuator transmission results in a cable tension of 1385 N given a motor torque of 2.42 Nm, which is larger than the required peak cable tension of 556 N. Additionally, for this torque, the linear speed of the cable is 69.1 cm/s, which is above the minimum target of 28.7 cm/s.

2.1.3 Planetary Gear System

Using R derived in the previous section, a planetary gear system was designed to amplify τ_{motor}. The system consists of a sun gear attached to the output of the motor, three planet gears connected to the pulley output through a carrier, and a ring gear attached to the actuator housing. Gear tooth number (N) is related to gear radius by π, the tooth pitch, pressure angle, addendum, and dedendum distance. However, these values do not need to be calculated with respect to gear reduction, since reduction is a ratio of tooth numbers. In order to physically fit the planet gears and sun gear within the ring gear, the following is used [58]:

$$N_r = 2N_p + N_s \tag{6}$$

where N_r, N_p, and N_s are the numbers of teeth for the ring, planet, and sun gears respectively. Further, the teeth numbers of the rotating elements, the sun and planet gears (the ring gear facilitates the rotation and is itself stationary), can be related to the speed reduction using

$$\frac{1}{R} = \frac{1}{2} * \frac{N_s}{N_s + N_p}. \tag{7}$$

From this, the teeth numbers were chosen as follows: N_s of 20 teeth, N_p of 40 teeth, and N_r of 100 teeth. Using these numbers and standard gear sizing constraints in SolidWorks (Dassault Systems, Vélizy-Villacoublay, France), the gear system was designed to approximately fit the 12.7 cm (5 in) diameter profile of the motor. A pitch angle of 0.558 rad (32°) and a pressure angle of 0.35 rad (20°) was chosen for higher force contact during actuator operation [59]. In order for the planet gears to act as the output, a carrier piece was designed to connect all three planet gears via steel screw and pressure-fit bearings. This piece attaches to the pulley through a ball bearing interface, which offloads lateral force from the drive system to surrounding metal housing pieces. Two mounting plates are attached to either side of the actuator assembly to further offload forces and facilitate linearity of the actuating elements. The full actuator assembly is shown in Figure 4.

The actuator pulley, housing, interfaces, and mounting plates were manufactured in-house from aluminum 6061 using CNC. Similarly, the planetary gear transmission was also manufactured in-house from the same material using wire EDM. Including the motors, the actuators weigh 1.55 kg each, and fully assembled, the ABX weighs a total of 6.4kg,

which is substantially less than most previous active devices while having higher assistive torque capability (Table 1).

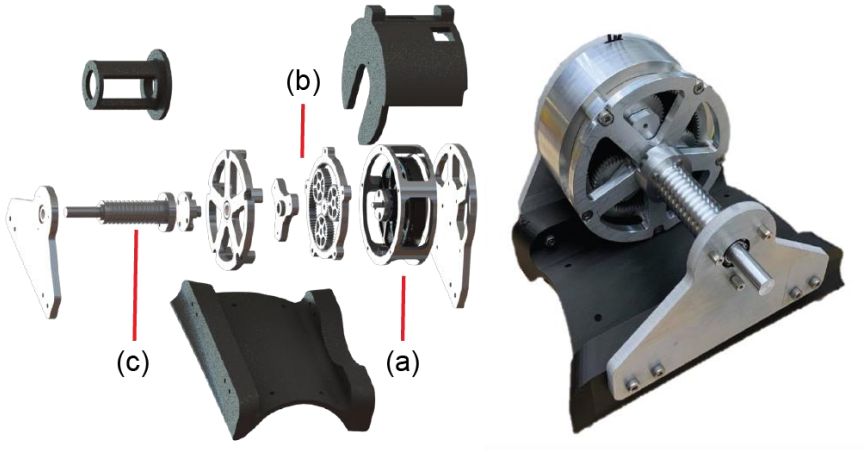

Figure 4 - The ABX thigh-mounted actuator is shown. The left subfigure shows an exploded view of the system, where (a) is the brushless DC motor driving the assembly and (b) is the 6:1 planetary gear reduction that transmits torque to the output pulley (c). Depicted above (a) is a plastic motor cover, which routes the motor windings and hall-effect sensor wires away from the cable line of action. Shown above (c) is the cable guide, which encapsulates the pulley in order to enforce proper spooling and prevent cable backlash. Below (b), the orthotic bracket which fastens the actuator to the thigh orthosis is shown. The assembled actuator is shown to the right of the exploded view.

2.2 Human Interface

2.2.1 Attachment Considerations

The exosuit attaches to the user's thighs and trunk using orthotic interfaces (Fillauer, Chattanooga, TN, USA) and a supportive modular vest (Condor Outdoor, Irwindale, CA, USA), respectively (Fig. 2A). The actuator mounting plates attach to the thigh orthosis via a custom-made mounting bracket. To fit the actuator mounting bracket to the thigh orthosis, the thigh orthosis was 3D scanned using a FaroArm (FARO, Lake Mary, FL, USA), and the mounting bracket was shaped using the generated point cloud.

Because this piece supports the weight and tension from the actuators and is of an irregular, difficult-to-machine shape, it was manufactured using a Markforged 3D printer (Markforged, Watertown, MA, USA) with Onyx material, giving it higher strength than other 3D-printable plastics at a light weight. Continuous stranded carbon fiber was inlaid around the major screw and rivet holes for actuator and orthotic attachment respectively, further reinforcing the piece.

Table 1 – Specifications of Back Assistive Devices

Device	Type	Mass (kg)	Trunk Extension Assistance (Nm)
Lamers *et al.* (2017)	P	2.0	12
Toxiri *et al.* (2018)	A	11.0	80
Zhang and Huang (2018)	A	11.2	100
Alemi *et al.* (2019)	P	4.5	-
Yong *et al.* (2019)	A	5.0	128
Heo *et al.* (2020)	A	10.5	80
Koopman *et al.* (2020)	P	6.7	50
ABX	**A**	**6.4**	**172***

P = Passive, A = Active. * represents peak extension torque at the start of the symmetric lift (see Chapter 3 Section 3.3.8)

2.2.2 Cable Routing and Plastic Components

To ensure proper spooling of the cable around the actuator pulley, the pulley was externally threaded with a pitch of 0.38 cm. This resulted in a maximum spooling length

of 79 cm. Additionally, a cable guide is attached axially around the pulley (Figure 4). This ensures the cable spools along the external threads by constraining radial travel using two plastic bars. After the actuator pulley, the cable is routed through the mechanical hard stops, which were made from wire rope clamps used to limit the maximum cable length the actuators can spool (Figure 2-A). This was used to prevent over-extending the user beyond an upright position in the case of unintended device actuation.

The cables are then routed through the glute cable guide to ensure that the cables do not slip around the user, which would degrade the lumbar assistive torque of the exosuit. This cable guide is adjustable for each user so that it sits approximately on the largest radius of the glutes maximus during lifting. Further, it attaches to the exosuit vest through mesh straps near the low back. The actuation cables then pass through the lumbar cable guide underneath the electronics housing all contained on the vest, which facilitates the crossing pattern of the cables. Finally, each cable attaches to the opposite shoulder via a carabiner mounted in series with the tension load cells (see Section 2.3.1). All of the cable guides were manufactured using an Ultimaker 2+ 3D printer with Ultimaker Tough PLA (Ultimaker, Utrecht, NL).

2.3 Sensor Integration and Controller

2.3.1 Sensor Suite

The ABX controller is executed using a sequential control loop deployed on an onboard Teensy 3.6 (PJRC) microcontroller (MC) at 200 Hz. The exosuit uses two load cells (Transducer Techniques, Temecula, CA, USA), one placed at each shoulder attachment in-line with the actuator cables to measure linear force provided to the user.

The load cell output voltages are amplified using two AD623 op-amps (Analog Devices, Norwood, MA, USA) and are each sampled once per control loop. An MPU9250 inertial measurement unit (IMU) (TDK, San Jose, CA, USA) is placed at the cervicothoracic junction, which estimates trunk orientation in real-time as a set of Euler angles updated by the built-in digital motion processor at 67 Hz. Two electronic speed controllers (ESCs) (Flipsky, Dongguan City, China) govern actuator operation using speed control based on serial commands from the MC over UART. The actuators are powered using two 22.2 V, 3600 mAh LiPo batteries (Venom Power, Rathdrum, ID, USA) wired in series. The load cells are powered using a separate 11.1 V, 800 mAh LiPo battery (Venom Power, Rathdrum, ID, USA). The MC, ESCs, load cell amplification circuit, and batteries are mounted in the electronics housing located along the user's thoracic spine (Figure 2-A).

2.3.2 Low-Level Controller and Finite State Machine

In order to autonomously assist the user, we implement a two-tier control system. Specifically, the mid-level finite state machine (FSM) detects the user mode throughout the lift and updates the control gains and desired cable tension (s_d) of the low-level force controller accordingly. The low-level control law (Figure 5) dictates the commanded motor velocity of each motor (ω_{cmd}) using the difference between s_d and the measured cable tension (s) from the corresponding load cell, the measured user trunk extension velocity (ω_t) from the IMU, and the control gains (k_s and k_h) as

$$\omega_{cmd} = k_s(s_d - s) + k_h\omega_t \,. \tag{8}$$

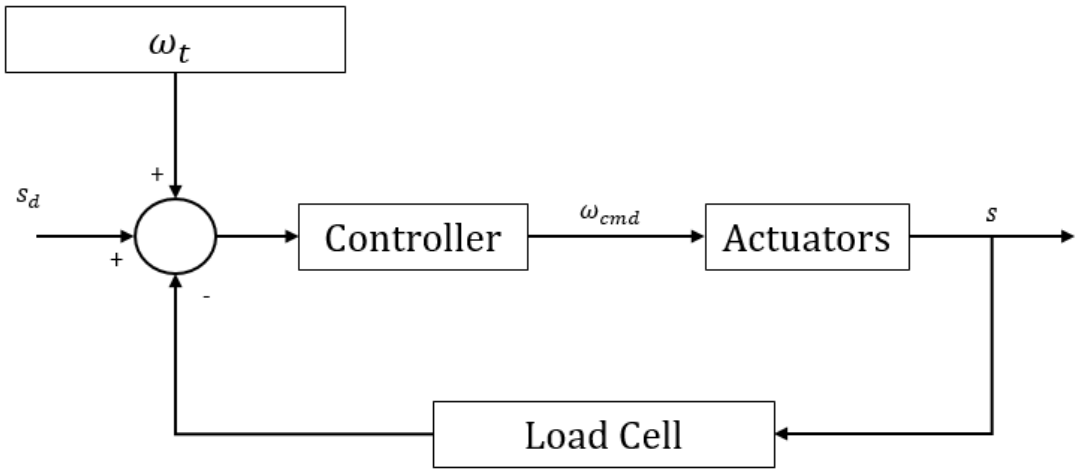

Figure 5 - Block diagram of the low-level controller. Trunk extension velocity and desired cable tension are fed into the low-level control law. This outputs a velocity command to the actuators, which induces cable tension. Using the Load Cells, tension is measured and fed back through the controller.

The first term in the control law is used to track the desired cable tension using the proportional gain, k_s. The second term is used to compensate for the movement of the user. This allows the cables to unspool as the user bends down towards the object and provides a convenient method for taking up the slack in the cable as the user lifts the object. This allows the proportional error term to be tuned with a much smaller gain as it is not needed for compensating for user movement, but rather for tracking the desired force using conventional servo control.

The magnitudes of k_s and k_h are hand-tuned for each user to optimize force tracking. Once tuned, these gains are autonomously varied during the lift depending on the user state detected by the FSM, shown in Fig. 4. The parameters θ_0 and θ_b are defined as the stand angle (the trunk angle measured by the IMU corresponding to when the user is in a neutral standing position) and bent angle (the trunk angle measured by the IMU that

occurs ~10° before the user reaches the bottom of the lift), respectively. These values are also calibrated per user before device operation. Hand-tuning of the control gains and FSM thresholds takes approximately 10 minutes per subject.

During operation, the FSM (Figure 6) transitions between states based on the measured trunk extension angle angle (θ_t) and trunk extension velocity (ω_t). Neutral Standing (State 0) is entered when the trunk extension angle is larger than the stand angle ($\theta_t \geq \theta_0$). During Neutral Standing, the FSM sets k_s and k_h to zero to disable operation of the actuators. The FSM transitions to Transparency Mode (State 1) from Neutral Standing once the trunk extension angle is less than the stand angle ($\theta_t < \theta_0$). During Transparency Mode, k_s is set to zero and k_h is updated to the tuned magnitude to allow transparent (open-loop zero force) tracking of the cables with the user's trunk motion. Once the user's trunk flexion reaches or exceeds the bent angle ($\theta_t \leq \theta_b$), the FSM transitions to Cable Pre-Tension (State 2). During Cable Pre-Tension, k_s and k_h are set to the previously tuned magnitudes and s_d is incremented from zero to the starting assistance force over a 500 ms period. This allows the actuators to preemptively remove slack from the cables and quickly ramp up to assistance while avoiding user discomfort, similar to the action of an elastic element. After tensioning the cables, the FSM transitions the low-level controller into Full Assistance (State 3) once the user's trunk extension velocity exceeds a predefined threshold (ω_{FA}). For this study, we fixed ω_{FA} at 1.2 rad/s (70 °/s) for all users. During Full Assistance, k_s and k_h remain at their tuned magnitudes to provide assistance according to the programmed desired force trajectory. Once the user's trunk extension angle exceeds the stand angle during Full Assistance, the FSM transitions back to Neutral Standing. Additionally, the FSM is programmed to transition to Transparency Mode if ω_t

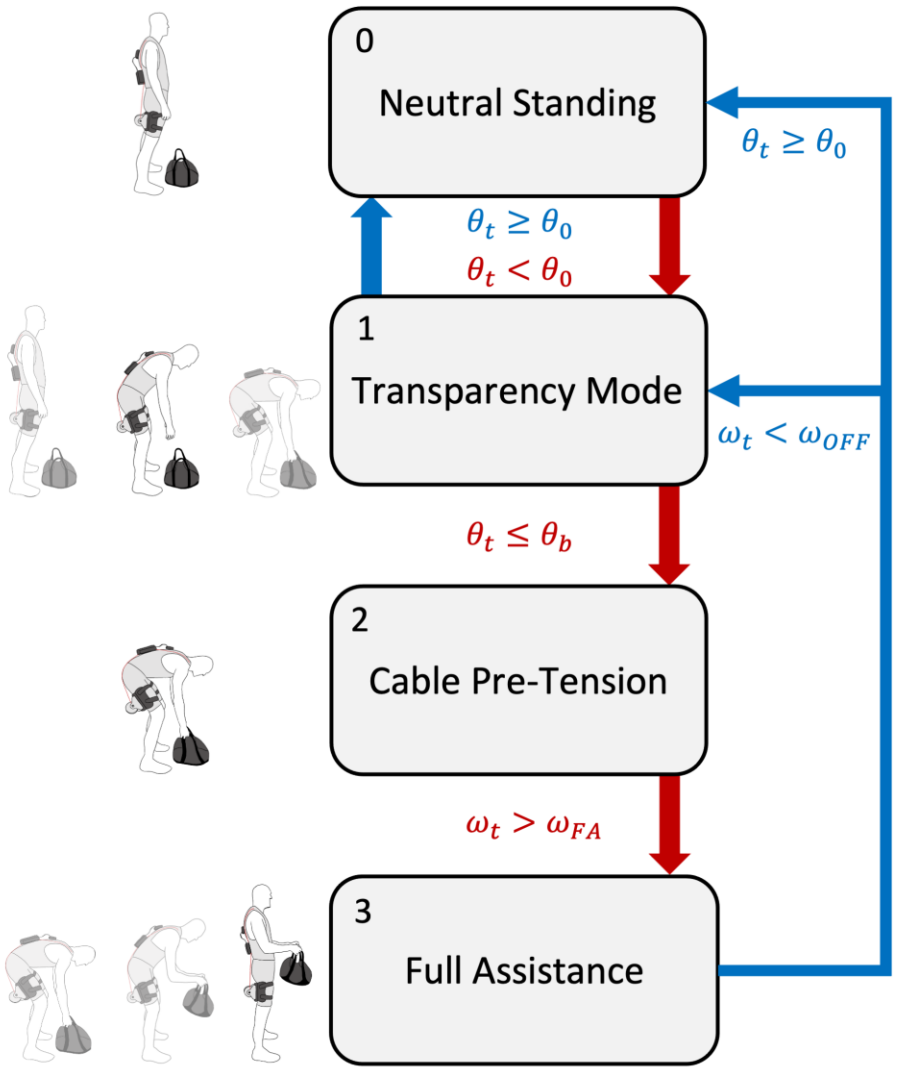

Figure 6 - The Finite State Machine (FSM) used to control the ABX is shown. When device operation begins, the user stands in neutral position (State 0). Once they begin to bend their trunk ($\theta_t < \theta_0$) the actuators slack or tension the cables based on the flexion/extension angle of the trunk (State 1) until the user bends down past the bent angle threshold ($\theta_t \leq \theta_b$). The user prepares to lift an object as the cables spool up until the desired assistive force is reached (State 2). Once this occurs, the user initiates full assistance (State 3) by beginning to lift so that their trunk flexion/extension angular velocity is greater than the set threshold ($\omega_t > \omega_{FA}$). Once the user is at the top of the lift and stops moving, the device returns to State 0. If the user stops in the middle of the lift and does not reach neutral standing, they enter State 1.

falls below a predefined threshold (ω_{OFF}) during Full Assistance as an additional safety feature. We fixed this threshold at 0.5 rad/s (30 °/s) for all users. Thus, the exosuit is completely autonomous, meaning that the system hardware is self-contained on the user

and that the controller does not require external information dictated by a separate operator (e.g., manual mode state transitions).

CHAPTER 3. HUMAN-EXOSUIT OUTCOMES STUDY AND BIOMECHANICS STUDY

3.1 Overview

The evaluation of the ABX consists of 3 main parts. First is an actuator validation on benchtop and on user. Second is the human-exosuit outcomes study that explores how ABX affects trunk muscle EMG during symmetric and asymmetric lifting of various weights, as well as the lumbar torque workspace of the device and how it affects user range of motion (RoM). Lastly, the third part details the early EMG results from the biomechanics study, a large-scale study designed to evaluate the ABX's effect on user biomechanics and trunk muscle EMG with varying assistance magnitudes.

Common among all the described evaluations is the maximum assistive force application of 25% of user bodyweight. While the ABX is capable of much greater force magnitudes, it was found in early development that magnitudes above 25% user bodyweight became uncomfortable when preparing to lift (FSM State Cable Pretension). For the weight of an average adult male, around 90.7 kg (200 lbs.) [60], the resulting cable force in each ABX cable is 111 N (25 lbs.) or 222N total across the a user's back. This is also in line with previous work on passive exosuits of similar structure from Lamers *et al.* that evaluated lifting at a peak elastic band force of 27% user bodyweight [30] and Abdoli *et al.* that assisted with around 200 N in the elastic elements across the back during lifting [34].

3.2 Exosuit Actuator Validation

3.2.1 Methods

To evaluate the performance of our actuators in providing assistive force, steady-state force tracking was evaluated during benchtop and on-subject conditions using the nominal desired force of 111 N (25 lbs.). During the benchtop condition, the actuator was mounted to a screwboard and connected to a tension load cell by a 100 cm nylon cable (approximate maximum cable length during lifting). Desired force was increased from 0 to 111 N over 500 ms and the resulting force was measured by the load cell at 200 Hz. The same protocol was performed using both the left-thigh and right-thigh actuators. Additionally, we tested the ABX assistance tracking performance while worn by a human subject lifting a 15.9 kg (35 lbs.) weighted bag. Similar to the benchtop condition, the desired force was increased from 0 to 111 N per cable over 500 ms during Cable Pre-Tension and commanded to a constant desired force of 111 N during Full Assistance.

3.2.2 Results

The steady-state force tracking error for the benchtop condition was computed as the root mean square error (RMSE) between the desired and measured cable force over the first two seconds after the cable reached 95% of the 111 N desired force. Similarly, the force tracking error for the on-subject condition was computed as the RMSE between desired and measured cable force during Full Assistance. The on-subject assistance was controlled using the autonomous FSM.

During the benchtop condition, the average assistance tracking RMSE was 2.4 N and 1.4 N for the left-thigh and right-thigh actuators, respectively. Figure 7 shows a representative trial during the on-subject condition. Similar to the benchtop condition, the

assistance tracking RMSE during the on-subject condition was 1.2 ± 0.4 N and 2.3 ± 0.8 N for the left-thigh and right-thigh actuators, respectively. In both conditions, the average tracking RMSE was less than 3% of the total desired force, demonstrating that the actuators accurately provided cable tension.

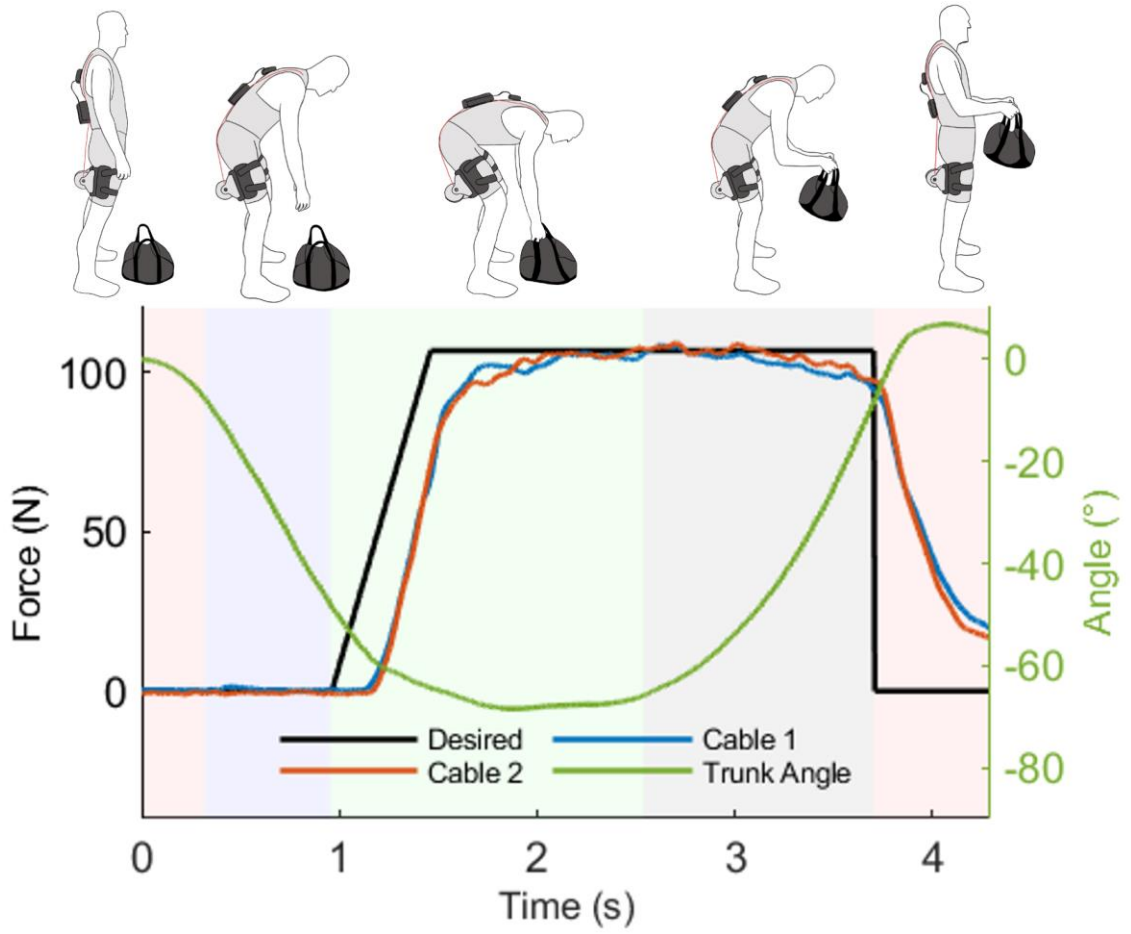

Figure 7 - A representative trial of the actuator performance during on-subject assistance is shown. The phases of the lift are characterized by the background colors on the plot. Desired force is the black profile, and tracking this profile are left and right actuators (blue and red). The flexion/extension angle of the user's trunk is shown in green. During Full Assistance, the actuators tracked the desired force of 111 N (25 lbs.) with an RMSE of 1.8 N.

3.3 Human-Exosuit Outcomes Study

3.3.1 Overview

We conducted a series of experiments to evaluate the effect of the ABX assistance on user outcomes. Specifically, we measured the change in EMG measurements of the trunk musculature compared to lifting without the exosuit to quantify the benefits of the ABX on reducing low back muscle effort. Additionally, we measured lumbar range of motion (RoM) with and without the exosuit to assess any penalties the ABX may have on the user's freedom of movement. Finally, we adapted a previously validated full-body OpenSim model [61]–[63] to quantify the assistive workspace of the exosuit with respect to the lumbosacral joint. This third analysis provided a high-fidelity characterization of the ABX's effect on the 3-DoF lumbosacral moments, relaxing the assumptions and limitations of previous back assistive device analyses, such as assuming constant device moment arms and planar lumbar movement [30], [52], [53]. Lumbar dynamics are reported as defined by the lumbosacral reference frame shown in Figure 2-B.

3.3.2 Muscle Activation Experiment: Methods

To evaluate the effects of ABX assistance on the user during lifting, we conducted a three subject (average age of 22.7 ± 0.6 years, mass of 79.1 ± 3.6 kg, and height of 1.79 ± 0.06 m) validation experiment approved by the Georgia Institute of Technology Central Institutional Review Board (H19276). Each subject provided informed consent prior to completing the experimental protocol, and none of the subjects had histories of low back injury or musculoskeletal disorders that would confound the results of this experiment. The participants lifted weighted bags using three techniques, which were labeled the symmetric (SYM), asymmetric 90° (ASYM90), and asymmetric 180° (ASYM180) techniques,

designed to vary the lumbar twist at the start and end of the lift (Figure 8). Each lifting technique consisted of lifting the weighted bag from the ground (~5 cm away from the user's feet) and placing it on a table with a height of 75 cm. The SYM technique consisted of sagittally lifting the weighted bag from a starting position directly in front of the user's feet and ending directly in front of the user. The ASYM90 technique involved lifting the weighted bag placed on the user's right side to enforce a 90° rotation at the start of the lift and placing the bag on the table directly in front of the user. Finally, the ASYM180 technique involved lifting the weighted bag placed on the user's right side and placing it on the table set on the left side of the user, inducing a 180° rotation from the start to end of the lift. Each participant completed five repetitions, lifting three different weighted bags of 6.8, 15.9, and 22.7 kg (15, 35, and 50 lbs., respectively) for the SYM and ASYM90 techniques and lifting a single weighted bag of 15.9 kg (35 lbs.) for the ASYM180 technique under two exosuit conditions. The exosuit conditions were: 1) NO EXO, in which the user completed the lifts without wearing the exosuit, and 2) EXO ASSIST, in which the exosuit actively provided 25% of the user's bodyweight evenly distributed between the cables during the upward portion of the lift, similar to the peak assistance force in a previous passive exosuit study [30]. Thus, each subject completed 70 lifting repetitions. Prior to completing the experimental conditions, participants were instructed to stand with feet shoulder-width apart and to stoop while lifting with a slight bend in the knees across lifting techniques. The movements were practiced across bag weights and lift techniques until the participants were comfortable with the movements and proper lifting technique was verified by the experimenters.

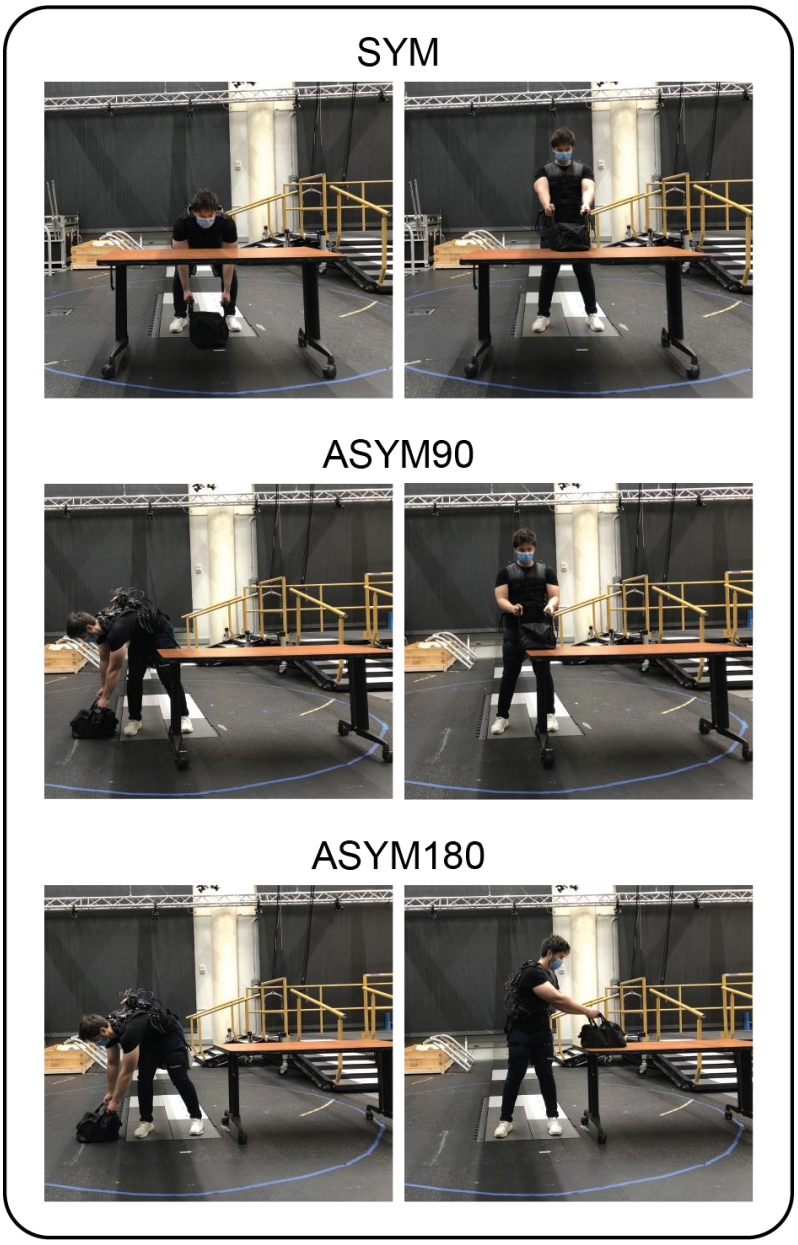

Figure 8 - The experimental setup is shown. The participants lifted weighted bags of 6.8, 15.9, and 22.7 kg (15, 35, 50 lbs.) from the ground to a 75 cm elevated table using varying lifting techniques. The symmetric (SYM), asymmetric 90° (ASYM90), and asymmetric 180° (ASYM180) lifts were tested to evaluate the effects of exosuit assistance across common lifting techniques of varying lumbar twist.

During each experiment, electromyography (EMG) data was collected using a Biometrics DataLINK DLK900 Data Acquisition System (Biometrics Ltd, Newport, UK) at 1000 Hz. Electrodes were placed on the left and right lumbar erector spinae (LLES and

RLES), left and right latissimus dorsi (LLD and RLD), left and right external obliques (LEO and REO), and rectus abdominis (RA) muscle groups. The electrodes were placed in accordance with SENIAM standards [64].

3.3.3 Muscle Activation Experiment: Data Analysis

EMG data of each trial were offset by the mean of the signal, filtered using a bandpass 30 to 300 Hz zero-phase fifth order Butterworth filter, rectified, and then lowpass filtered with a 6 Hz zero-lag fifth order Butterworth filter. The root mean square muscle activation (rEMG) was computed over a three second period for each repetition. The rEMG data for each channel (one per muscle group) of the EXO ASSIST trials were then normalized to the corresponding averaged rEMG data of the NO EXO condition. The EMG results are presented as the percent change in rEMG of the EXO ASSIST conditions relative to the corresponding NO EXO conditions (average ± 1 standard error of the mean (SEM)). One subject's data for the LLES and RLES groups were excluded due to malfunction caused by the cable action interfering with the electrodes. Also, for the same subject, EMG malfunction on the RA group occurred during two repetitions of the ASYM90 6.8kg lifts which were also discarded. The rEMG for the LLES and RRES muscles was averaged over two subjects.

3.3.4 Muscle Activation Experiment: Results

Figure 9 shows the relative change in rEMG of the EXO ASSIST condition compared to the NO EXO condition for each lift technique and weighted bag mass. Across all technique types and bag weights, trunk extensor muscle (LLES, RLES, LLD, RLD) rEMG was decreased. Specifically, with regard to the LLES and RLES groups, large rEMG

reductions were observed in symmetric lifting across bag weights (44.0 ± 3.88% L and 46.5 ± 3.39% R for 6.8kg, 36.9 ± 8.21% L and 37.9 ± 2.25% R for 15.9kg, 31.6 ± 15.6% L and 30.1 ± 8.38% R for 22.7kg). Regarding ASYM90 lifting, reductions were also observed, but to a lesser extent (32.0 ± 6.48% L and 21.0% ± 20.4% R for 6.8kg, 6.73 ± 6.48% L and 14.7 ± 17.6% R for 15.9kg, 1.5 ± 6.04% L and 17.8 ± 10.4% R for 22.7kg). For the ASYM180 condition, similar reductions are observed (18.0 ± 15.5% L and 10.2 ± 16.9% R for 15.9kg). The LLD and RLD groups also experienced generally large reductions across all conditions and weights, except for the ASYM90 technique with 6.8kg bag weight.

As for the flexor muscles (LEO, REO, RA), decreases of activation were observed, except for the LEO group at the 6.8kg bag weight, where activation increased by 12.8 ± 9.93%, during symmetric lifting. Regarding ASYM90, increases of the REO and RA groups of 8.39 ± 9.69% and 32.6 ± 34.8%, respectively, for the 6.8kg weight were observed. Another increase occurred for the RA group of 3.79 ± 5.99% during the 22.7kg lift of the same technique type. During the ASYM180 technique, RA also increased by 5.31 ± 0.74%. Other than these increases, trunk flexor muscle rEMG was generally decreased across technique types and bag weights.

3.3.5 RoM and Lumbar Torque Workspace Experiment: Methods

On a separate day from the muscle activation experiment, one participant (age of 23 years, mass of 81.6 kg, and height of 1.75 m) returned to complete a second experimental protocol to collect kinematic data to evaluate user range of motion changes when using the ABX. The second protocol consisted of seven lifting repetitions of the 15.9

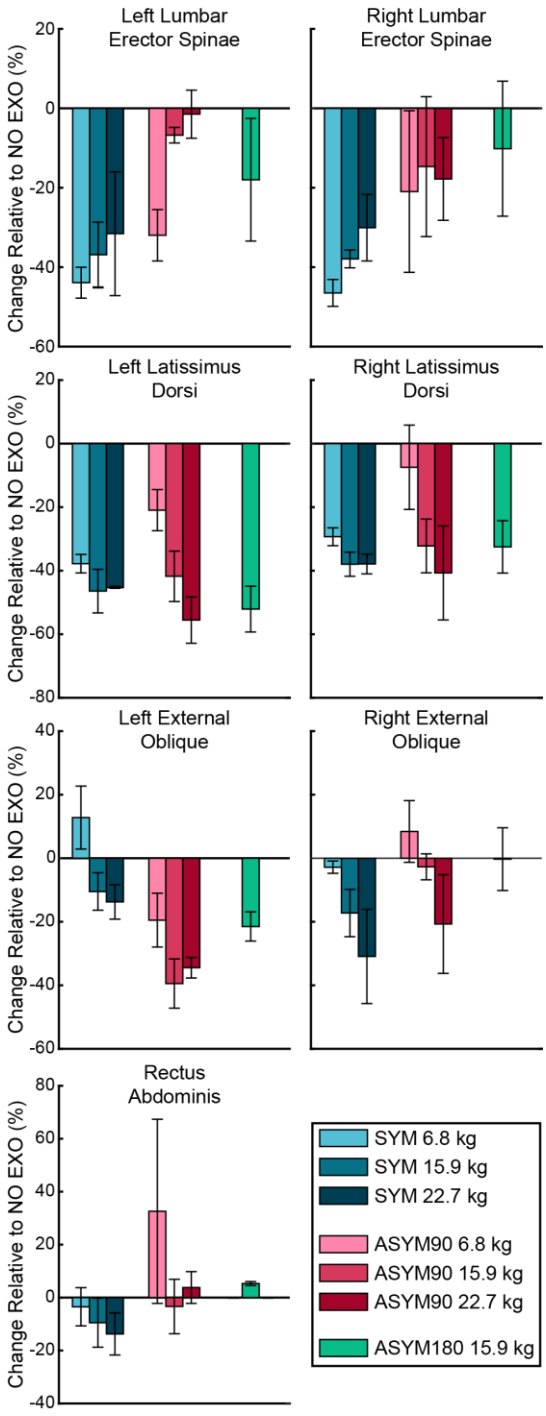

Figure 9 - The resulting muscle activations while using the ABX are shown as the relative change to those measured without wearing the device (NO EXO). All muscle activations were measured using surface electromyography. The results are presented for each tested bag weight during the symmetric (SYM), asymmetric 90° (ASYM90) and asymmetric 180° (ASYM180) lifts as the average change in RMS muscle activation ± 1 SEM.

kg (35 lbs.) bag using each of the three prescribed lifting techniques (Figure 8). During this protocol, the NO EXO and EXO ASSIST conditions were repeated, as well as a SLACK condition, in which the exosuit was worn while unpowered with slack in the cables during the entire lift. During this experiment, whole-body motion capture data was collected using a 32-camera Vicon motion capture system (Vicon, Oxford, UK) at 200 Hz. Retroreflective markers were used to collect kinematic data of the feet, shanks, thighs, pelvis, trunk, arms, and hands. Additionally, 6-axis force data was collected using two Bertec force plates (Bertec, Columbus, Ohio, USA) at 1000 Hz to mark the start and end of the lift.

3.3.6 RoM and Lumbar Torque Workspace Experiment: Exosuit OpenSim Model

To compute the resulting lumbar RoM and assistive torque workspace of the ABX, we modified the OpenSim Lifting Full-Body (LFB) model [63], a musculoskeletal model validated for analyzing the lumbar spine during lifting movements, to include musculotendon actuators representative of the two actuation cables of the ABX (Figure 2-B). The start and end points of the modeled cables were fixed using the ABX thigh and shoulder attachment locations as measured using motion capture markers during a subject-specific calibration trial. Additionally, the modeled cables were guided along the trunk and pelvic bodies using massless, frictionless wrapping surfaces to mimic the constraints of the exosuit cable guides.

3.3.7 RoM and Lumbar Torque Workspace Experiment: Data Analysis

The motion capture and force plate data were lowpass filtered using a zero-lag fifth order Butterworth filter with a cutoff frequency of 6 Hz and 20 Hz, respectively. The start of the lift was marked when the weighted bag was fully removed from the starting force

plate. Similarly, the end of the lift was marked when the weighted bag first contacted the ending force plate. We then computed the lumbar RoM and ABX assistive torque workspace using OpenSim [61], [62]. The motion capture data of the 58-marker full-body marker set was used to scale the anthropometry, inertial properties, and exosuit cable attachment points of the modified LFB model to fit that of the individual participant using the OpenSim Scale Tool. The generalized joint coordinate trajectories of the scaled model for each lifting trial were then computed using the built-in OpenSim Inverse Kinematics Tool, which minimizes the weighted sum of least squares between the experimental and modeled markers as a function of the generalized coordinates of the model. Using these joint trajectories, the lumbar RoM for each trial was computed as the difference between the maximum and minimum trunk angle with respect to the sacrum through the lift in the flexion/extension, axial rotation, and lateral bending DoFs (shown in Figure 2-B).

We then used the OpenSim Muscle Analysis Tool to compute the ABX moment arms of the scaled model with respect to the L5/S1 joint. The Muscle Analysis tool defines the effective moment arm ($r_\theta \in \mathbb{R}$) between a DoF and musculotendon actuator (a) as the ratio of torque induced at the DoF (τ_θ) with respect to the tension of the musculotendon actuator (s_a) given the set of generalized coordinates of the model (q) [65] as

$$r_\theta(q) \triangleq \frac{\tau_\theta}{s_a}. \tag{9}$$

With this formulation, the solver computes the effective moment arms using two assumptions: 1) the path of the musculotendon actuator (l) is fully described by the generalized coordinates of the model $\left(l = l(q)\right)$, and 2) the tension in the musculotendon

actuator is uniform and the transform between spatial forces and tension is linear. Using these assumptions, the effective moment arm of the musculotendon actuator is computed using the generalized forces $\left(f(s)\right)$ defined by the model geometry, the joint-specific geometric coupling matrix (C_θ), and by fixing s to unit tension (s_o) [65]:

$$r_\theta = \frac{f^T C_\theta}{s_0}. \tag{10}$$

The assistive torque workspace of a given biological DoF (W_θ) was then computed using the definition show in (5), the effective moment arms of the exosuit cables (R_θ), and the interval between the minimum (S_{MIN}) and maximum (S_{MAX}) cable tensions that can be generated by the exosuit:

$$W_\theta(q) = \left\{R_\theta^T(q)S \mid S \in [S_{MIN}, S_{MAX}]\right\}. \tag{11}$$

Additionally, we defined the maximum restorative torque (J_θ) of the exosuit as the maximum assistive torque about a given biological joint that can be generated in the direction of the velocity of the generalized coordinate for the given joint of interest, calculated as

$$J_\theta \triangleq \begin{cases} \max\left(W_\theta(q)\right) & if\ \dot{q}_\theta > 0 \\ \left|\min\left(W_\theta(q)\right)\right| & if\ \dot{q}_\theta < 0 \\ 0 & otherwise \end{cases} \tag{12}$$

3.3.8 RoM and Lumbar Torque Workspace Experiment: Results

The resulting RoM results are shown in Table 2. Lumbar flexion RoM increased by 19.5%, 33.7%, and 6.3% during the SLACK condition and by 33.1%, 39.1%, and 19.2% during the EXO ASSIST condition compared to the NO EXO condition for the SYM, ASYM90, and ASYM180 techniques, respectively. Additionally, the EXO ASSIST condition increased the axial rotation RoM by 0.3° during the ASYM90 technique but reduced the axial rotation RoM by 9.4° during the ASYM180 technique compared to the NO EXO condition. Similarly, for the EXO ASSIST condition, lateral bending RoM increased by 7.7° during the ASYM90 technique but decreased by 3.1° during the ASYM180 technique compared to the NO EXO condition.

Table 2 – Lumbar Range of Motion

	SYM		
	NO EXO	SLACK	EXO ASSIST
Flexion / Extension	50.7 ± 5.0°	60.6 ± 3.9°	67.5 ± 4.4°
Axial Rotation	11.0 ± 2.5°	4.5 ± 0.6°	5.2 ± 1.7°
Lateral Bending	6.6 ± 3.4°	3.8 ± 2.4°	5.9 ± 4.9°

Table 2 – Lumbar Range of Motion Continued

	ASYM90		
	NO EXO	SLACK	EXO ASSIST
Flexion / Extension	43.2 ± 3.4°	57.7 ± 1.9°	60.1 ± 1.8°
Axial Rotation	10.1 ± 1.5°	13.6 ± 1.9°	10.4 ± 2.2°
Lateral Bending	30.2 ± 2.4°	27.9 ± 2.0°	37.9 ± 1.7°
	ASYM180		
	NO EXO	SLACK	EXO ASSIST
Flexion / Extension	50.0 ± 2.4°	53.0 ± 2.4°	59.4 ± 4.2°
Axial Rotation	29.7 ± 1.8°	29.7 ± 3.1°	20.3 ± 3.7°
Lateral Bending	48.3 ± 3.2°	38.8 ± 5.4°	45.2 ± 5.0°

The average lumbosacral extension moment arm of the ABX cables during the SYM lift was 6.73 ± 0.06 cm. Similarly, the averaged extension moment arm was 6.74 ± 0.16 cm and 6.69 ± 0.07 cm during the ASYM90 and ASYM180 lifts, respectively. The axial rotation moment arms varied substantially between cables, resulting in average values of -0.73 ± 0.05 cm, -0.57 ± 0.06 cm, and -0.5 ± 0.07 cm for the left cable and 0.60 ± 0.04 cm, 0.84 ± 0.02 cm, and 0.81 ± 0.05 cm for the right cable during the SYM, ASYM90, and ASYM180 techniques, respectively. Similarly, the average lateral bending moment arms

were 1.68 ± 0.09 cm, 0.33 ± 0.18 cm, and 0.44 ± 0.16 cm for the left cable and -1.45 ± 0.05 cm, -2.00 ± 0.14 cm, and -1.75 ± 0.08 cm for the right cable during the three lifting techniques.

The effective workspace of the ABX with respect to the lumbosacral joint over the kinematic trajectory for each of the three lifting techniques is shown in Figure 10. The maximum restorative lumbosacral torque induced by the device varied throughout the lift. At the beginning of the lift, the maximum restorative torque was 172.4 ± 4.2 Nm, 165.4 ± 1.5 Nm, and 163.8 ± 4.2 Nm in extension, 4.1 ± 0.9 Nm, 16.2 ± 0.3 Nm, and 18.3 ± 3.1 Nm in axial rotation, and 16.4 ± 1.4, 61.6 ± 1.7 Nm, and 63.4 ± 5.1 Nm in lateral bending for the SYM, ASYM90, and ASYM180 techniques, respectively.

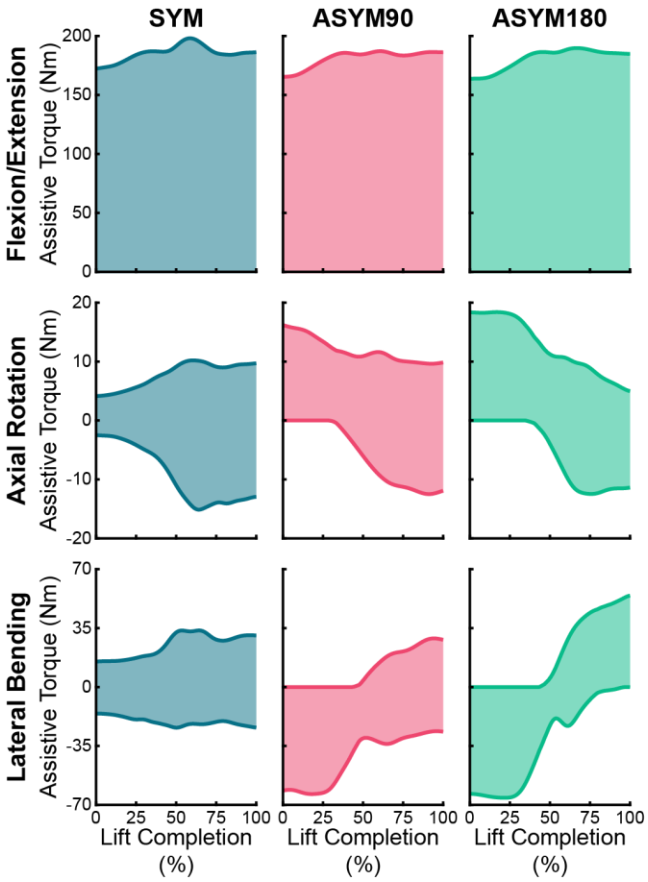

Figure 10 - The averaged assistive workspace of the exosuit, defined as the set of torque values the exosuit can induce on a given degree of freedom for a set of generalized model coordinates, is shown for each lumbosacral degree of freedom (rows) and lifting technique evaluated in our study (columns). The depicted time series start at the bottom of the lift and end when the user placed the weighted bag on the table.

3.4 Biomechanics Study

3.4.1 Overview

Due to the promising results of the human-exosuit outcomes validation experiment, an expanded study was planned and conducted to more fully characterize the biomechanical effects of the ABX on users through EMG, motion capture, and musculoskeletal modelling through OpenSim [61], [62]. This comprises a larger

experimental population of greater human subject variability. Further, we explore a greater variety of assistance conditions as well as varied assistance in either cable during asymmetric lifting. In this section, the methods, data analysis, and results for EMG outcomes of three subjects of this study will be analysed and discussed.

3.4.2 Methods

The initial experimental population of the biomechanical evaluation consists of three subjects (average age of 22.3 ± 2.1 years, mass of 75.1 ± 14.5 kg, and height of 1.75 ± 0.04 m, right-handed, two males and one female). The protocol was approved by the Georgia Institute of Technology Central Institutional Review Board (H19276), and each subject provided informed consent prior to completing the experimental protocol. No subjects had histories of previous low back injury or musculoskeletal disorders that would confound the results of the experiment.

The subjects lifted a 15.9 kg weighted bag using the same SYM, ASYM90, and ASYM180 conditions shown in Figure 8. Additionally, a condition in which the assistive force applied to the user is varied between cables (70% assist on left shoulder, 30% on right), asymmetric 90° varied (ASYMV90), was evaluated. Each lifting technique consisted of lifting the weighted bag from a Bertec force plate next to the subject's feet and placing it on another force plate on a raised platform normalized to subject knee height. The experimental setup is shown in Figure 11. The evaluated assistance conditions were based on proportions of user bodyweight applied evenly between both actuator cables ranging from 10% to 25% in 5% increments as well as the NO EXO condition (five conditions total). The ASYMV90 condition was evaluated over the 10% and 20%

bodyweight assistances only. The assistance magnitudes were randomized per lift technique, while the NO EXO conditions were completed before the subject initially equipped the ABX. Each permutation was performed for 7 repetitions. Thus, each full experiment consisted of 119 lifts total. A survey using the Borg Rating of Perceived Exertion Scale [66] was administered at the end of every lift permutation to judge the user's perception of the assistance magnitudes. On a separate day prior to each experiment, subjects participated in a 45-minute training session involving 15 minutes of practicing lifts of the SYM, ASYM90, and ASYM180 techniques and 30 minutes of wearing the ABX and experiencing the assistance conditions over the techniques.

Muscle activation data was collected using two Delsys Trigno Quattro Sensors (Delsys Incorporated, Natick MA, USA) at 1000Hz. One was placed on the posterior trunk with the four leads being placed on the LLES, RLES, LLD, and RLD muscles and the other placed on the anterior trunk with three leads on the LEO, REO, and RA groups. The electrodes were placed according to SENIAM guidelines [64]. Whole-body motion capture data was collected using a 32-camera Vicon motion capture system (Vicon, Oxford, UK) at 200 Hz, and retroreflective markers were used to collect kinematic data of the feet, shanks, thighs, pelvis, trunk, arms, and hands. Additionally, 6-axis ground reaction force data was collected using two Bertec force plates (Bertec, Columbus, Ohio, USA) at 1000 Hz under each of the subject's feet. Two other force plates were used to mark the start and stop of the lift. At the beginning of every experiment, max voluntary contractions (MVC) of the desired muscle groups were obtained using standard techniques [67]–[69].

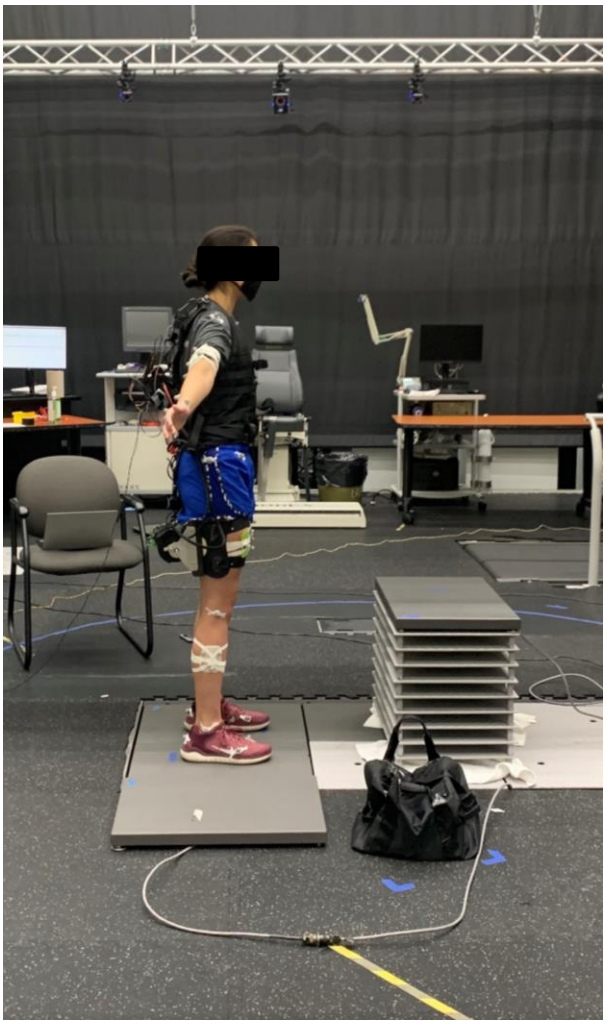

Figure 11 – Experimental Setup for the Biomechanical Evaluation Experiment. The subject, equipped with the ABX and instrumented with retroreflective markers and EMG sensors, stands on force plates during all lift permutations. The lift starts when the weighted bag leaves the start force plate (next to the user's feet) and ends when the bag touches the end force plate (on the raised platform).

3.4.3 EMG Data Analysis

EMG data of each trial were offset by the mean of the signal, filtered using a bandpass 30 to 300 Hz zero-lag fifth order Butterworth filter, rectified, and then lowpass filtered with a 6 Hz zero-phase fifth order Butterworth filter. The EMG signals were 1) windowed between the start (as the weighted bag begins to leave the start force plate) and

stop (as soon as the weighted bag contacts the end force plate) of the lift, 2) integrated (iEMG), 3) resolved to peak values (pEMG), and 4) averaged over the seven repetitions respective of each analysis type. The EMG results are presented as percent change in iEMG or pEMG of the different assist conditions relative to the corresponding NO EXO conditions. Each subjects' results are reported individually. The standard deviation of the repetitions per assistance magnitude are also shown.

For subject 2 (SUB2), the LLD group was excluded due to improper EMG capture during the experiment. Also, the LEO group during the SYM 25% BW condition was averaged over four repetitions instead of seven. For subject 3 (SUB3), the ASYMV90 condition was not conducted due to experimental time constraints. Also, for SUB3's RLD group, three reps were discarded from the SYM 10% BW condition, two reps were discarded from the SYM 15% BW condition, and two reps discarded from the SYM 25% BW condition. For the LEO group, one rep was discarded from the SYM 10% BW condition and one rep was discarded from the SYM 15% BW condition. All exclusions were due to the repetitions having high noise and large motion artifacts corrupting the signal.

3.4.4 Results: Subject 1

The iEMG results for SUB1 (Subject 1, 91.85 kg, 1.8 m) are shown in Figure 12. For the SYM lifts, trunk extensor and flexor muscle activations largely decreased as assistance magnitude increased. However, activation increased for the LLES at low assistances respective of NO EXO (i.e. +35.9 ± 18.6% for 10% BW, +16.2 ± 17.8 for 15% BW, and +10.7 ± 11.1% for 20% BW). Conversely, for the ASYM90 lifts, increasing

assistance did not cause decreasing muscle activation except for the RLES group (-15.2 ± 9.4% for 10% BW, -19.2 ± 6% for 15% BW, -23 ± 13.3% for 20% BW, and -21.7 ± 5.7% for 25% BW). The trunk flexor muscles and LLES generally saw iEMG increases, while the LLD and RLD group were largely unaffected as assistance increased. The trunk flexor groups experienced decrease in activation in the ASYMV90 condition as assistance increased from 10 to 20% especially in the RLES group (-26.1 ± 5.4% for 20% BW). Increasing assistance also decreased LLES activation, but activation was increased by both magnitudes. Increases were also experienced in the extensor muscles, specifically the LEO and RA groups (+2.4 ± 9.8% and +13.4 ± 11.4% for 20% BW respectively). The ASYM180 condition induced the overall greatest increase in LLES activation (+75.5 ± 16.2% for 20% BW), increase in RLD activation (+53.5 ± 13.8% for 10% BW), and decrease in RLES activation (-39 ± 5.6% for 25% BW). Also, regarding this condition, trunk flexor muscle groups generally increased activation for all assistance conditions except for the RA group during 15% BW (-0.7 ± 7.3%).

The averaged pEMG results for SUB1 are shown in Figure 13. Across lift techniques and assistance magnitudes, RLES, LLD, RLD, and LEO muscle groups decreased in activation. Specifically for the SYM technique at 25% BW, large pEMG reductions were observed for LLES (-24.6 ± 17.3%), RLES (-31.9 ± 10.2%), LLD (-46.3 ± 14.9%), RLD (-45.7 ± 6.4%), LEO (-49.3 ± 8.8%), RA (-23 ± 11.8%) groups. However, the LLES group experienced activation increase at lower assistance magnitudes of 10 and 15% BW. Under the ASYM90 condition, LLES, REO, and RA groups all experienced activation increases (max at +33.2 ± 35% for 20% BW, +37.7 ± 29.7% for 20% BW, and +15.9 ± 39.7 for 25% BW for LLES, REO, and RA respectively). However, the RLES,

LLD, RLD, and LEO all experienced large reductions (~35 – 42%) under the 15 and 25% BW conditions. The ASYMV90 condition exhibits the most consistent pEMG reduction across the muscle groups. Conversely, the ASYM180 technique shows reductions in the RLES, LLD, RLD, LEO, and RA groups (~2 – 60% reduction over assistance magnitudes) and increases in the LLES and REO groups (~6–38% increase over assistance magnitudes).

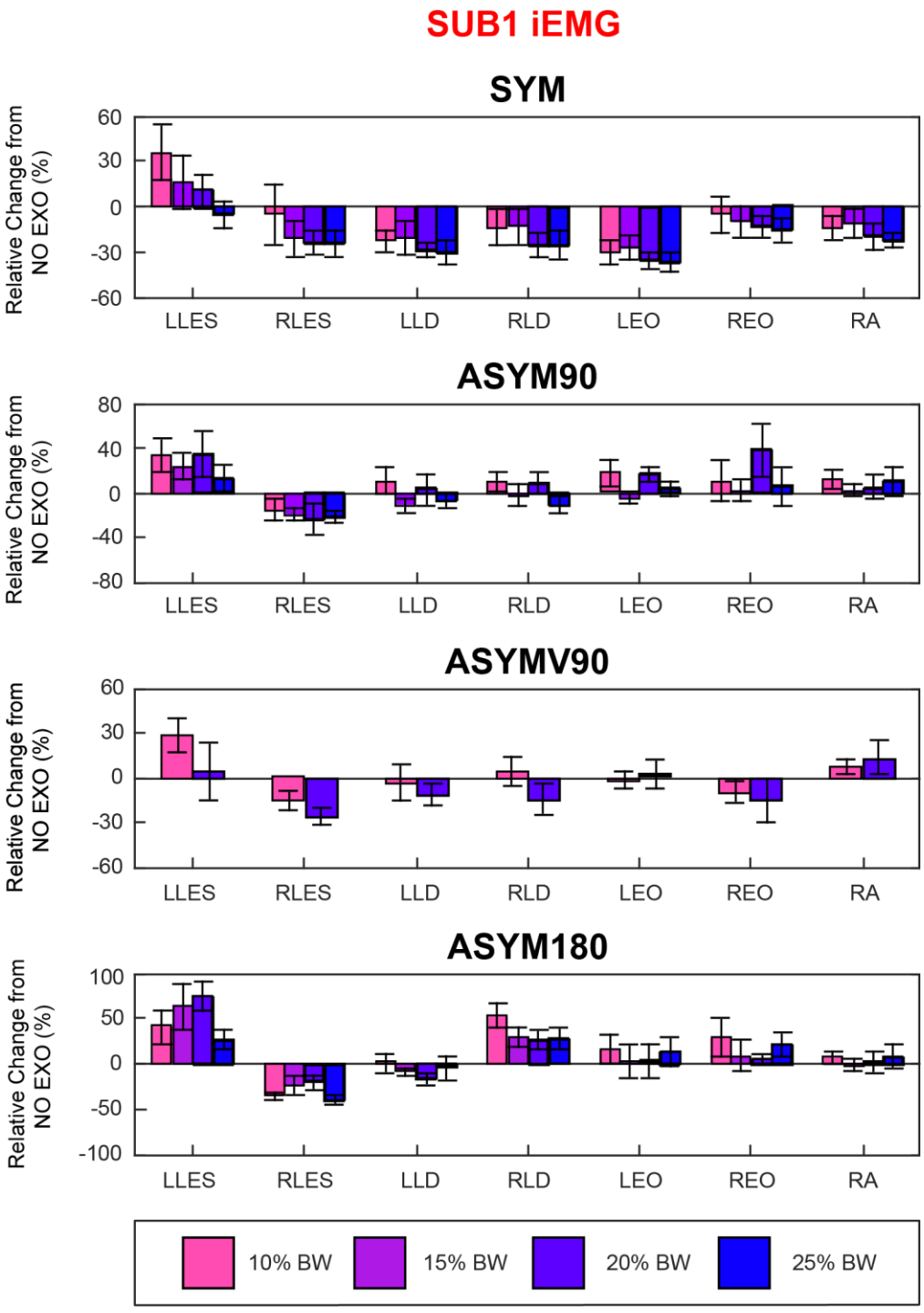

Figure 12 – SUB1 iEMG Results.

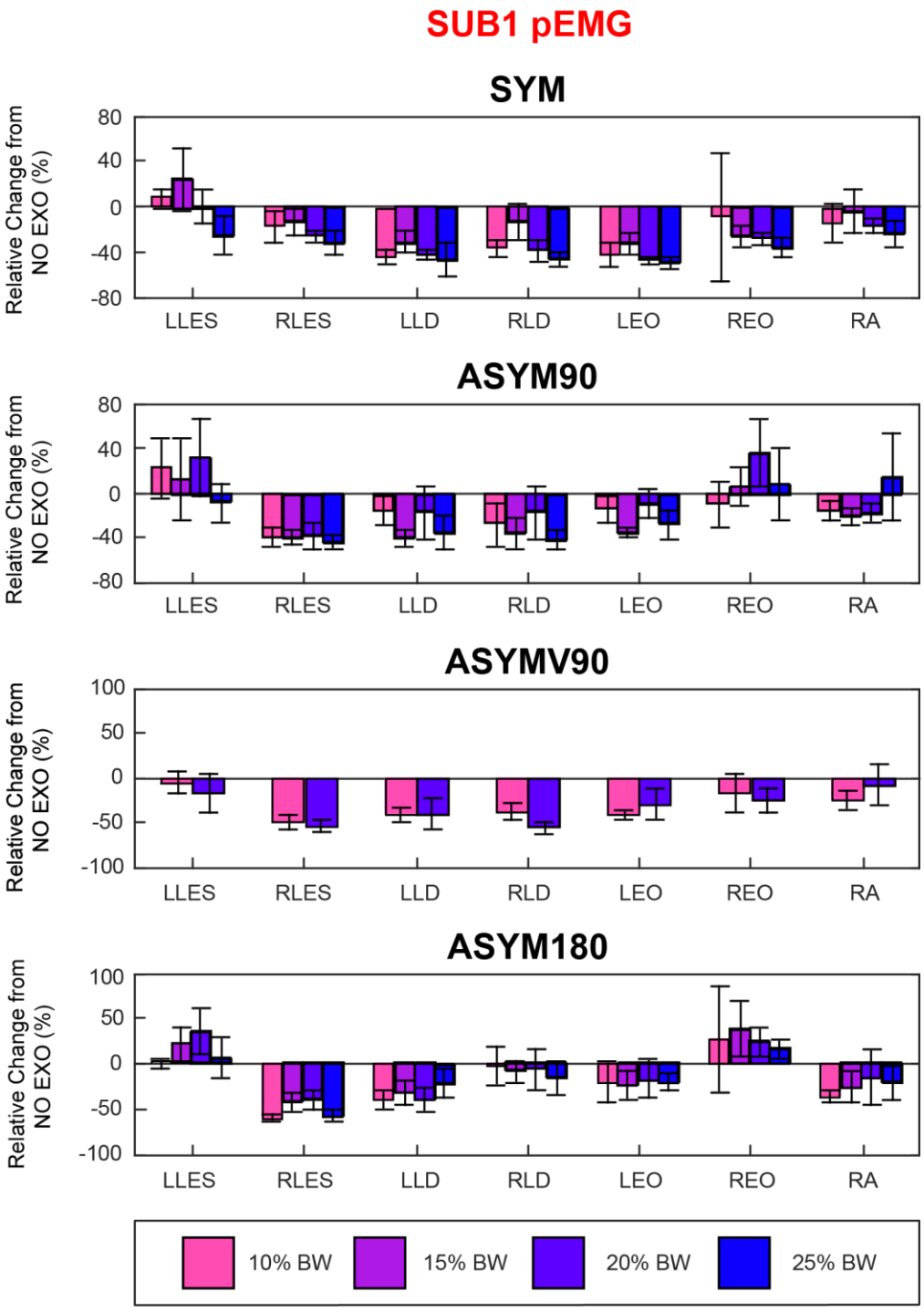

Figure 13 – SUB1 pEMG Results.

Regarding the Borg scale survey from this subject, perceived exertion decreased across each lifting technique as assistance increased (15-16 for NO EXO, 14-15 for 10% BW, 13-14 for 15% BW, 13-12 for 20% BW, and 12 for 25% BW). Also, the duration of each of the NO EXO lifts (1.4 ± 0.06s for SYM, 1.23 ± 0.5s for ASYM90, and 1.35 ± 0.1s for ASYM180) was found to be less than that of the four assistance conditions averaged together for each technique (1.52 ± 0.1s for SYM, 1.63 ± 0.07s for ASYM90, 1.74 ± 0.02s for ASYMV90, and 1.72 ± 0.1s for ASYM180).

3.4.5 Results: Subject 2

The iEMG results for SUB2 (Subject 2, 67.4 kg, 1.7 m) are shown in Figure 14. For the SYM condition, the LLES and RLES were slightly affected by assistance (+5.2 ± 4.7% to -8.3 ± 7%), while RLD experienced large decreases (up -35.6 ± 4.7% at 15% BW). At the same time, the LEO and REO groups experienced iEMG increases (up to +18 ± 11.5% at 20% BW and +26.1 ± 14.6% at 20% BW respectively). During the ASYM90 technique, the LLES group was largely unaffected, while the RLES group saw iEMG increases across assistance magnitudes (up to +18. ± 11% at 15% BW). All other groups experienced iEMG reductions. The ASYMV90 technique saw both the LLES and RLES groups increase (up to +16.1 ± 9.7% at 10% BW and +28.8 ± 15.9% at 10% BW respectively), while all other groups displayed iEMG reduction (-17 to -47%) except for LEO at 10% BW (+5.9 ± 17.3%). Similar results were observed for the ASYM180 technique as the trunk flexor muscles and RLD showed large iEMG reductions (-25.9 to -60.5%). The LLES group experienced smaller reductions for the 10%, 15%, and 20% BW conditions (-10.5 ± 6.4%, -16.4 ± 7.4%, and -6.2 ± 4.6% respectively), but experienced

iEMG increase at 25% (+4.0 ± 9.9%). The RLES group was largely unaffected (± 5 to 9% depending on assistance magnitude).

Shown in Figure 15 are the pEMG results for SUB2. During the SYM technique, LLES, RLES, RLD, and RA showed pEMG decrease (-3% to -28%), while LEO and REO increase activation (+19% to +40.3%). The ASYM90 condition shows large reductions in the RLD, LEO, REO, and RA groups (-10.1% to -68.7%), while activation increases were exhibited in the RLES group (+29.6 ± 26.3% at 25% BW). In the ASYMV90 condition, pEMG reductions are shown in all muscle groups except for the RLES group. The same is true for the ASYM180 technique in which large decreases were experienced for the RLD, LEO, REO, and RA groups (-21.9% to -65.2%) and slight pEMG reductions were experienced in the LLES group (-20.4 ± 6% at 15% BW). RLES saw slight activation increases (up to +6.9 ± 8.3% at 20% BW).

For the SUB2 Borg scale survey, the NO EXO conditions were perceived to require slightly less exertion (9 on the scale) than the ABX assistance conditions (10-11). Regardless of the assistance magnitude, SUB2's perception of exertion largely remained constant. The duration of the NO EXO lifts (1.6 ± 0.1s for SYM, 1.8 ± 0.1s for ASYM90, 2.1 ± 0.2s for ASYM180) was found to be only slightly less than (if not equal to) that of the four assistance conditions averaged together for each technique (2.0 ± 0.1s for SYM, 1.9 ± 0.1s for ASYM90, 2.1 ± 0.07s for ASYMV90, and 2.1 ± 0.1s for ASYM180).

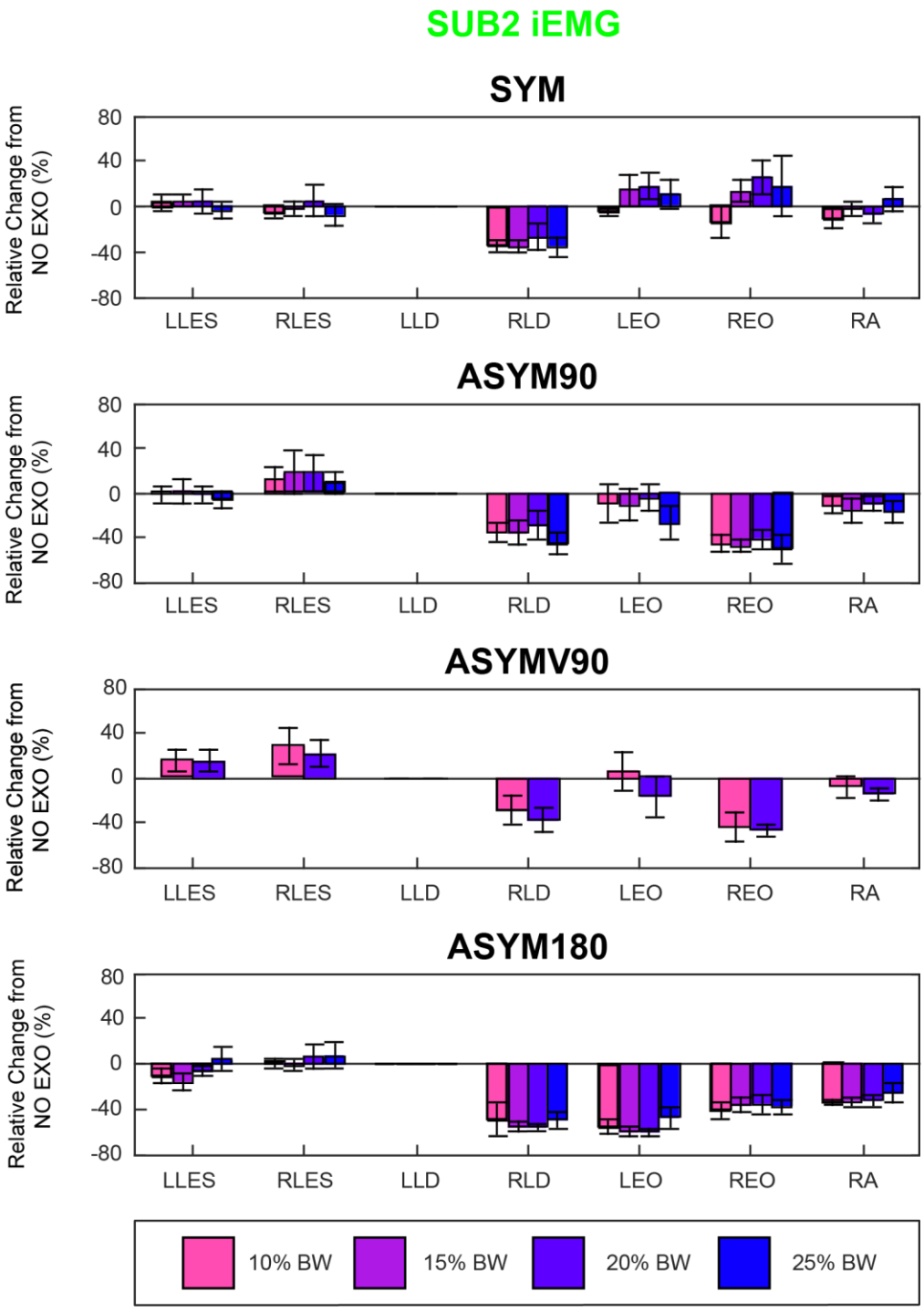

Figure 14 – SUB2 iEMG Results.

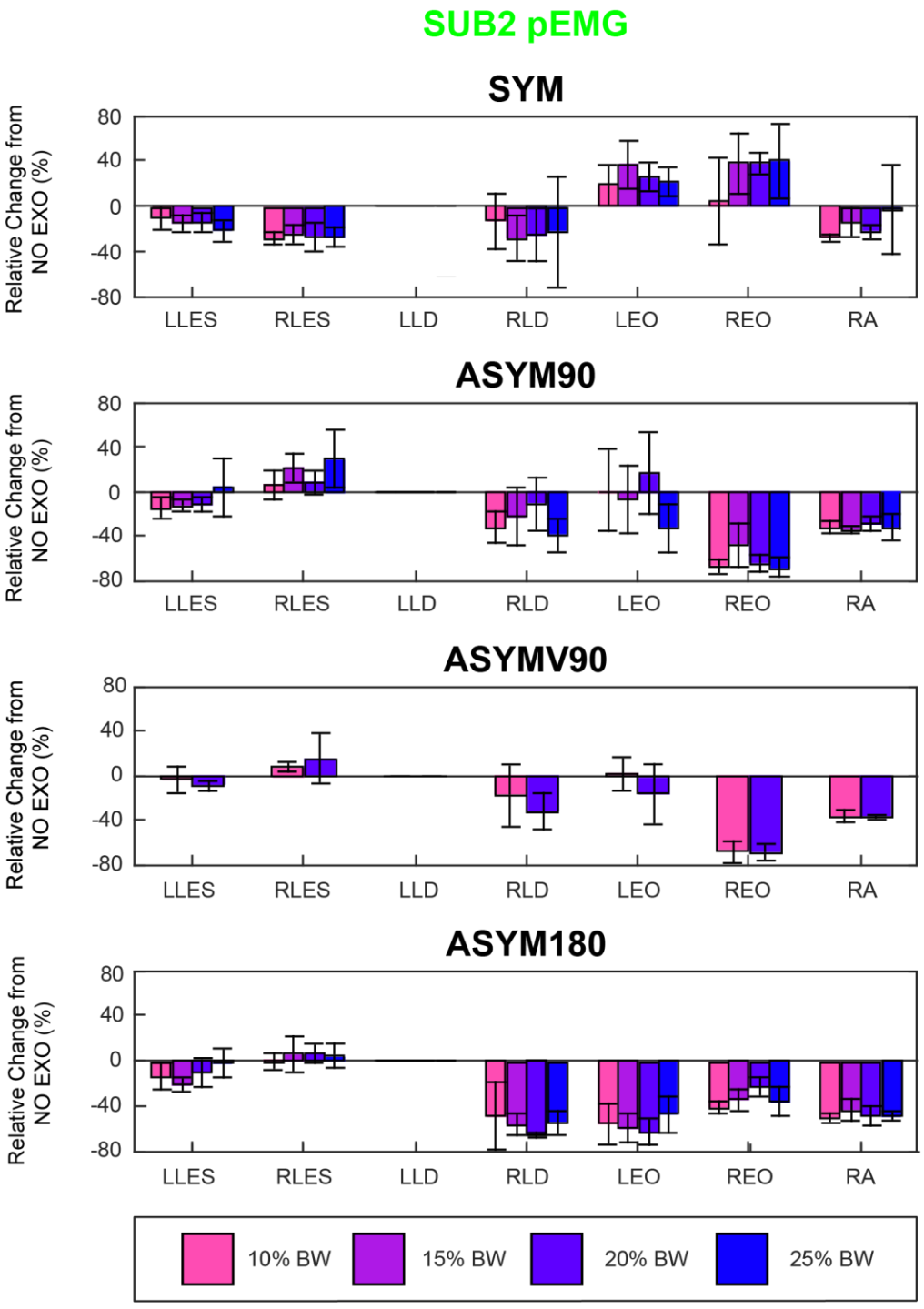

Figure 15 – SUB2 pEMG Results.

3.4.6 Results: Subject 3

The iEMG results for SUB3 (Subject 3, 67.4 kg, 1.73 m) are shown in Figure 16. Regarding the SYM technique, iEMG reductions are shown for both trunk flexor and extensor groups (LLES: -35.5 ± 5.2%, RLES: -25.9 ± 8.6%, LLD: -19.3 ± 9.9%, RLD: -33.8 ± 10.6%, LEO: -8.5 ± 15.3%, REO: -14.7 ± 16.4%, and RA: -28.5 ± 8.4%, all at 20% BW assist). Greater magnitude reductions were observed for the ASYM90 condition (LLES: -52.7 ± 14.1% at 20% BW, RLES: -30.2 ± 16.4% at 25% BW, LLD -31.3 ± 13.4% and RLD: -47.1 ± 6.8% at 15% BW, LEO: -19.2 ± 22.7% at 25% BW, REO: -30.0 ± 12.6% and RA: -52.6 ± 4.9% at 15% BW assist). The trend mostly continues into the ASYM180 condition, however the iEMG of the LLES and RLES groups are reduced to a lesser extent, and the LEO group increases activation at 25% BW (+9.2 ± 22.7%).

Next, the pEMG results for SUB3 are displayed in Figure 17. In symmetric lifting, pEMG activation increases are observed for the RLD (+16.2 ± 69.9% for 10% BW and +58.8 ± 24.8% for 15% BW) and LEO groups (+27.8 ± 40.6% for 20% BW and +24.6 ± 47.9% for 25% BW). Because the iEMG data does not reflect this, these high peak EMG values could be due to noise and motion artifacts. The REO group was mostly unaffected, while all other muscle groups' activations (LLES: -44.5 ± 10.2% and RLES: -37.3 ± 13.1% at 20% BW, LLD: -38.5 ± 5.7% at 15% BW, and RA: -52.1 ± 3.9% at 20% BW) are largely decreased. In the ASYM90 condition, the pEMG of all muscle groups are reduced except for RLES at 15% BW (+5.1 ± 31.3%). The same holds true for the ASYM180 condition, except the pEMG of LLES at 10 and 20% BW are both increased (+8 ± 20.9% and +0.1 ± 15.2% respectively).

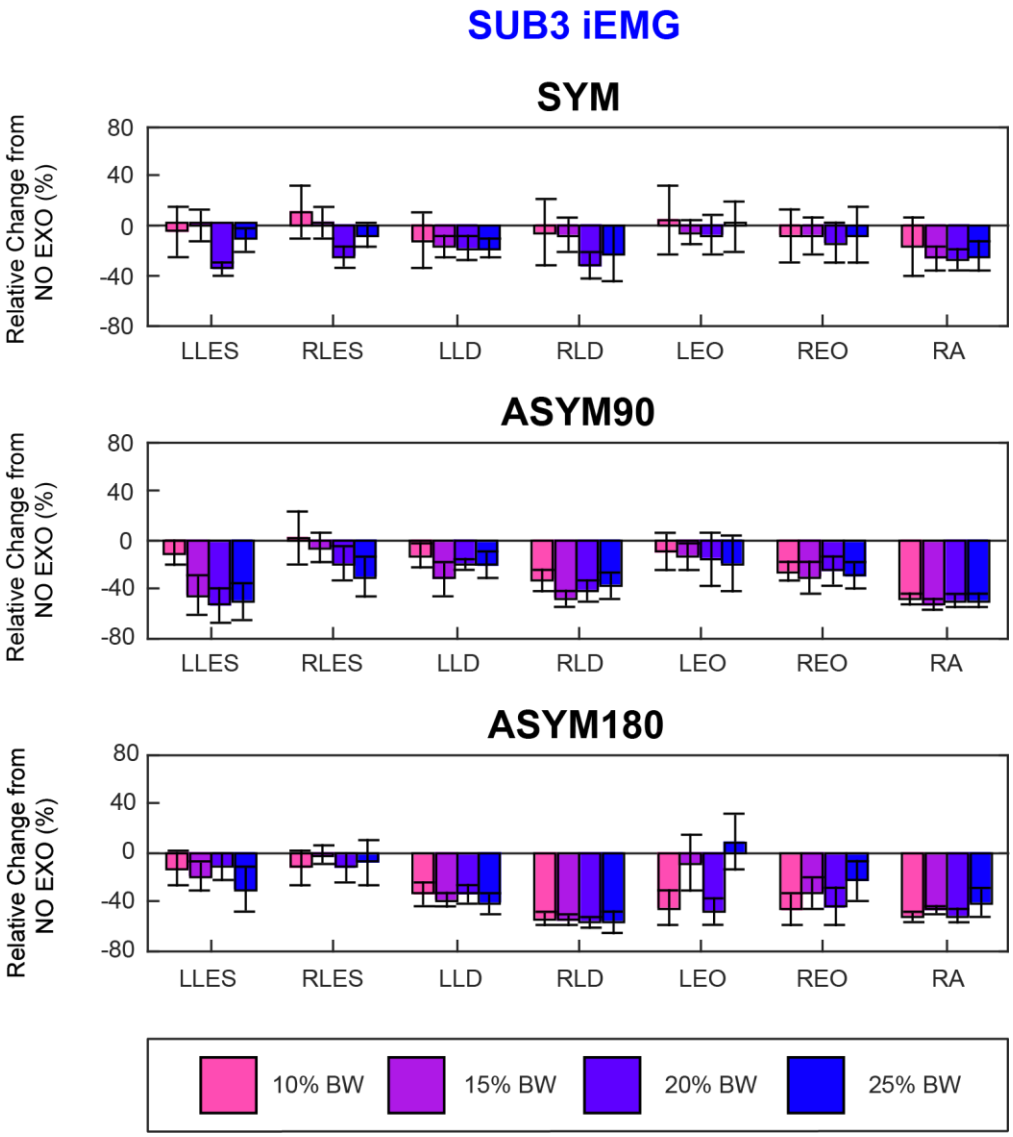

Figure 16 – SUB3 iEMG Results.

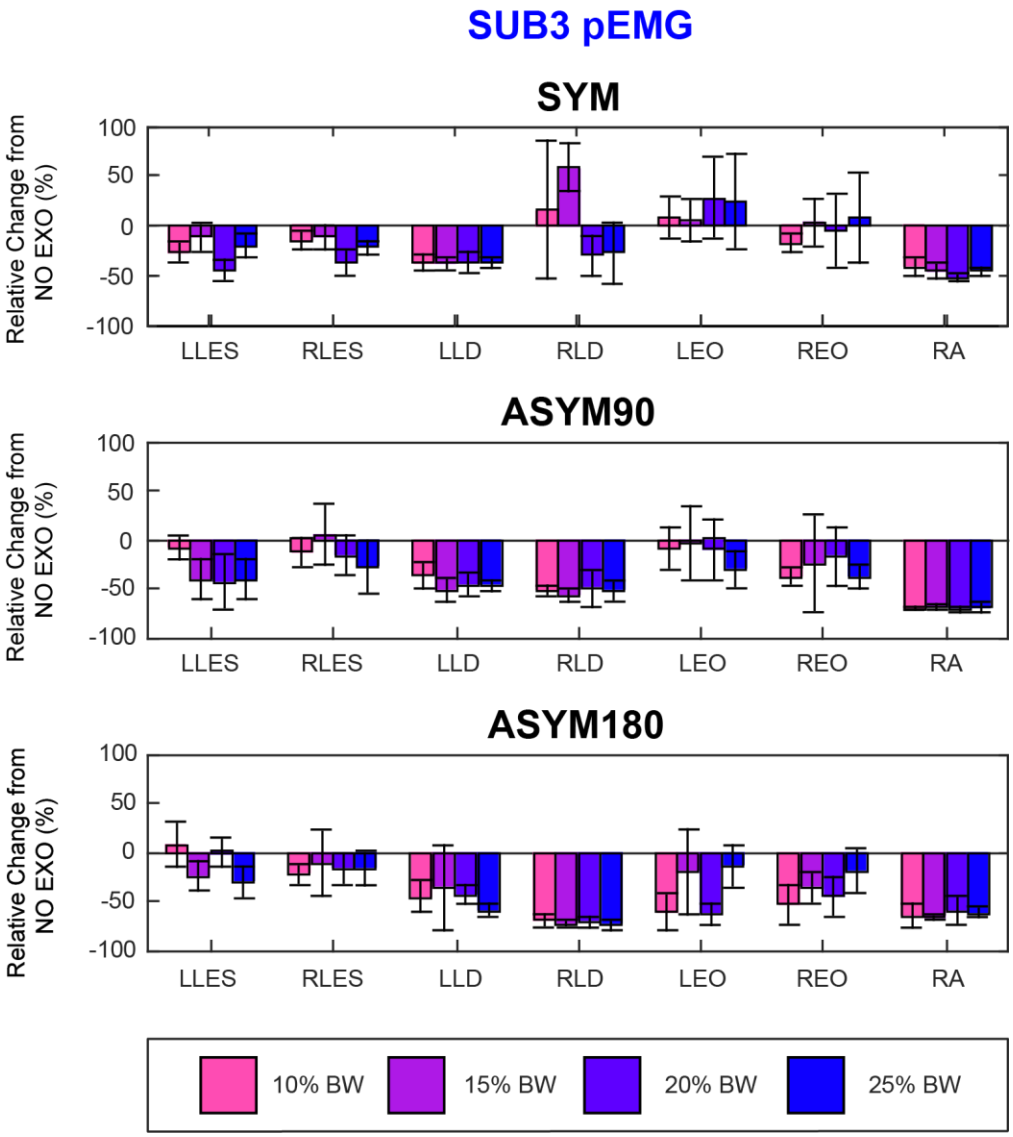

Figure 17 – SUB3 pEMG Results.

The Borg survey results for SUB3 show that all NO EXO conditions were rated as 11 (fairly light work). As assistance was applied, the lifts were perceived as slightly more strenuous (12) then progressively less strenuous as assistance application increased to 25% BW (10-11). Therefore. there was no significant change in the user's perception of the work regardless of assistance magnitude. The duration of the NO EXO lifts (1.8 ± 0.1s for SYM, 1.9 ± 0.3s for ASYM90, 1.8 ± 0.1s for ASYM180) was found to be very close to

that of the three assistance conditions averaged together for each technique (1.9 ± 0.1s for SYM, 1.8 ± 0.1s for ASYM90, and 1.7 ± 0.1s for ASYM180), resulting in, at most, a 0.1s difference between each respective technique.

CHAPTER 4. DISCUSSION AND CONCLUSION

4.1 Human Exosuit Outcomes

This thesis presented the design, realization, and human-subject validation of the ABX, an active, cable-driven back assistive device designed for realistic lifting conditions. We designed the ABX to provide active assistance across all DoFs of the lumbar spine while preserving the user's original range of motion during symmetric and asymmetric lifting.

From the human-exosuit outcomes experiment, we show that the ABX can decrease lumbar erector spinae rEMG ranging from 9.7% to 45.3% on average across bag weights and lifting techniques without coactivation for torso flexors. We also show that the reductions in lumbar muscle activation during symmetric lifting are comparable to those reported in previous active back exoskeleton studies (~25 to 40% in previous studies) [37]–[40], outperforming the results of passive exosuits (~14 to 29%) [29]–[31] due to the net positive work provided by the ABX. This result demonstrates that the flexible, cable-driven actuation of the ABX maintains lumbar assistance benefits compared to previous rigid exoskeletons. Further, the flexible nature of the ABX allowed our study to expand the investigation of active lumbar assistance effects on asymmetric lifting with up to 180° of rotation, which previous active devices restrict the user from performing. During the ASYM90 and ASYM180 techniques, the ABX reduced lumbar erector spinae muscle activation by an average of 15.6% and 14.1%, respectively. These results are slightly lower in magnitude than passive exosuit results in the literature (24 to 30%) [31], [34]; however, this is likely due to differences in the specific lifting conditions, making direct comparisons

challenging. Regardless, the results of the study show that the ABX provides benefits in lumbar muscle activation during symmetric lifting comparable to state-of-the-art active exoskeletons but generalizes those benefits beyond the operational workspace of these prior devices.

To characterize the assistance torque delivered to the lumbosacral joint by the exosuit, we adapted a previously validated OpenSim model to include the ABX cables as musculotendon actuators. From this model, we computed the effective moment arms and assistance torque workspace achieved by our device during the three lifting techniques. Interestingly, the average extension moment arm ranged from 6.69 cm to 6.74 cm among the lifting techniques with little variance throughout the lift (Fig. 8). This demonstrates that the lumbosacral extension moment arm of the exosuit remained mostly constant through a wide range of lifting asymmetry, which validates the constant extension moment arm assumption common to previous back assistive devices in the literature [30], [52], [53]. Additionally, the resulting lumbosacral extension moment arms of our OpenSim analysis were smaller than originally assumed; however, they are approximately 50% larger than the moment arms of the erector spinae muscles reported in comparable musculoskeletal models [63], [70], demonstrating the increased mechanical advantage of the ABX compared to the human musculoskeletal system with respect to the lumbosacral joint.

Using these computed moment arm trajectories and the peak force of our actuators, we computed the assistive torque workspace of each lumbosacral rotational DoF (Fig. 8). Though we implemented a control reference signal of constant force regardless of lift technique, trunk extension, and bag weight to validate the ABX in this study, future research will include using these workspaces to design optimized assistance trajectories as

influenced by changes in lumbosacral joint demands across varying tasks. Additionally, we quantified the maximum restorative torque at each lumbosacral DoF using the assistive torque workspaces. The maximum extension assistance of our device is substantially larger than previous active back exosuits (Table 1), providing the potential to explore novel magnitudes of actuator assistance, especially given the likely need for increased assistance with increased biological joint demand from varying conditions (i.e., changes in object weight).

We also quantified the user's lumbar RoM during the three investigated lifting techniques in this study to validate that the ABX did not limit the user's lumbar RoM. The largest reduction in lumbar RoM of 9.4° between the EXO ASSIST and EXO OFF condition occurred in axial rotation during the ASYM180 technique. Interestingly, this reduction in axial rotation did not occur during the SLACK condition, suggesting that this reduction in RoM was likely caused by the user's acceptance of the device assistance, not from restrictions caused by wearing the device itself. The RoM experiment did not result in other evidence that the ABX reduced lumbar RoM during symmetric or asymmetric lifting techniques.

4.2 Biomechanics Experiment – Early EMG results

Following the promising results from the initial study, we show integrated EMG and peak EMG data of three subjects (SUB1, SUB2, SUB3) from the large-scale biomechanics study. While SUB1 experienced considerable iEMG decrease in SYM lifting, the ASYM conditions proved more variable. Further, observing the pEMG from SUB1 shows more consistency in activation decrease. Across the board, only the RLES muscle group showed

consistent pEMG or iEMG decrease. SUB1 lifted the fastest out of the three subjects and perceived the most benefit from the device (through Borg Perceived Exertion [66]). SUB2 experienced mostly consistent pEMG and iEMG activation decreases of the LLD and torso flexor muscles, but the lower lumbar muscles rarely experienced considerable activation decrease. SUB2 lifted slower than SUB1 and perceived the nearly the same exertion level with or without the ABX. SUB3 had the most consistent large decreases of all muscle groups throughout pEMG and iEMG analysis. SUB3 lifted at around the same speed as SUB2 during the NO EXO conditions, but was slightly faster during assistance. SUB3 also perceived little-to-no change in exertion when using the ABX.

From these results, it can be indicated that there is variability in the operation of the ABX across users of differing anatomy. For example, SUB1, being taller and heavier than both SUB2 and SUB3, might require different force application methods to assist the trunk extensor and flexor muscles more effectively. However, even though SUB2 and SUB3 were of similar height, weight, and build, their results are markedly different. It could be that, overall, more training and practice with the suit is necessary to fully accept assistance from the ABX regardless of anatomy. Following this, more complex control methods could also be explored to optimize force application to users. Biological EMG activation profiles or joint torque profiles could be implemented to assist the user more naturally instead of through simple ramp inputs. Thankfully, this work has been initially explored with the biological torque workspace (Figure 10).

The preliminary results from the biomechanics experiment show that the ABX can reduce trunk flexor and extensor pEMG and iEMG activation during symmetric and asymmetric lifting. Moreover, the original hypothesis, the ABX is able to reduce risk

factors of LBP in symmetric and asymmetric lifting, is initially supported by the EMG and biomechanics results from the human-exosuit outcomes experiment and the initial EMG results from the biomechanics study. However, more insight for this hypothesis will be obtained through full biomechanical analysis of the full subject cohort with determining muscle forces and joint loading of the L5/S1 during lifting using OpenSim [61], [62] and CEINMS [71].

4.3 Limitations

There are a few limitations in the design that should be considered for improving the usefulness of the ABX. One limitation is that, based on our OpenSim model, the exosuit cables have a smaller extension moment arm than other devices that use similar actuation methods (e.g., Abdoli *et al.* reported an extension moment arm of 22 cm using a glute plate [34]). It is likely that the mechanical advantage relative to the trunk extensor muscle groups of our device can also be increased using similar geometric structures. Regardless, the ABX still causes substantial reduction in trunk extensor EMG with the current geometry. Another limitation of our device is that multiple users reported that the actuators were heavy on the thighs and resulted in discomfort near the end of the experimental protocol. The design choice to mount the actuators on the user's thighs was made to reduce exosuit weight bared on the lumbar spine and to minimize friction in cable routing; however, the actuator placement can be reconsidered in future modifications to improve comfort. Finally, given that the maximum actuation force of the ABX is likely above the user's comfort limit [72], the actuator assistance capability and weight can likely be reduced.

Our studies also included experimental limitations. All experiments showcased in this thesis consisted of small subject counts (N=3 or N=1) making it difficult to conclude significance of results. Additionally, the evaluation of human-subject lumbar benefit was limited to muscle activation results based on trunk EMG. Though this approach has been the standard for evaluating back assistive devices, it does not provide direct insight into the effect the ABX has on known LBP risk factors, such as compressive and shear loading in the lumbar joints [73]. Again, this will be explored with biomechanical analysis of the results from the full biomechanics study dataset.

4.4 Conclusion

The ABX was designed to provide powered assistance to users in symmetric and asymmetric lifting while staying lightweight and unobtrusive. Early validation studies show that the ABX is effective in this regard by reducing the activation of trunk extensor muscles tied to development of LBP [11], maintaining user range of motion, and providing assistive torque over the 3 DoFs of the lumbar spine. This is further evaluated in a larger scale biomechanical analysis of the ABX for which initial pEMG and iEMG reductions for trunk extensor and flexor muscles are observed. While there is variability in the effectiveness of assistance per subject, the ABX can reduce trunk EMG activation in SYM and ASYM conditions, partially validating the original hypothesis. Because the ABX is an adaptable device, multiple new avenues of control can be explored to improve device operation and assistance application to all possible users.

REFERENCES

[1] D. Hoy, P. Brooks, F. Blyth, and R. Buchbinder, "The Epidemiology of low back pain," *Best Pract. Res. Clin. Rheumatol.*, vol. 24, no. 6, pp. 769–781, Dec. 2010, doi: 10.1016/j.berh.2010.10.002.

[2] H. Yang, S. Haldeman, M.-L. Lu, and D. Baker, "Low Back Pain Prevalence and Related Workplace Psychosocial Risk Factors: A Study Using Data From the 2010 National Health Interview Survey," *J. Manipulative Physiol. Ther.*, vol. 39, no. 7, pp. 459–472, Sep. 2016, doi: 10.1016/j.jmpt.2016.07.004.

[3] A. Wu *et al.*, "Global low back pain prevalence and years lived with disability from 1990 to 2017: estimates from the Global Burden of Disease Study 2017," *Ann. Transl. Med.*, vol. 8, no. 6, Mar. 2020, doi: 10.21037/atm.2020.02.175.

[4] J. N. Katz, "Lumbar Disc Disorders and Low-Back Pain: Socioeconomic Factors and Consequences," *JBJS*, vol. 88, no. suppl_2, pp. 21–24, Apr. 2006, doi: 10.2106/JBJS.E.01273.

[5] J. K. Freburger *et al.*, "The Rising Prevalence of Chronic Low Back Pain," *Arch. Intern. Med.*, vol. 169, no. 3, pp. 251–258, Feb. 2009, doi: 10.1001/archinternmed.2008.543.

[6] "Back injuries prominent in work-related musculoskeletal disorder cases in 2016 : The Economics Daily: U.S. Bureau of Labor Statistics." https://www.bls.gov/opub/ted/2018/back-injuries-prominent-in-work-related-musculoskeletal-disorder-cases-in-2016.htm (accessed Feb. 26, 2020).

[7] J. I. Kuiper, A. Burdorf, J. H. A. M. Verbeek, M. H. W. Frings-Dresen, A. J. van der Beek, and E. R. A. Viikari-Juntura, "Epidemiologic evidence on manual materials handling as a risk factor for back disorders:a systematic review," *Int. J. Ind. Ergon.*, vol. 24, no. 4, pp. 389–404, Aug. 1999, doi: 10.1016/S0169-8141(99)00006-2.

[8] P. Coenen *et al.*, "The effect of lifting during work on low back pain: a health impact assessment based on a meta-analysis," *Occup. Environ. Med.*, vol. 71, no. 12, pp. 871–877, Dec. 2014, doi: 10.1136/oemed-2014-102346.

[9] D. B. Chaffin and K. S. Park, "A longitudinal study of low-back pain as associated with occupational weight lifting factors," *Am. Ind. Hyg. Assoc. J.*, vol. 34, no. 12, pp. 513–525, Dec. 1973, doi: 10.1080/0002889738506892.

[10] U. Latza, A. Pfahlberg, and O. Gefeller, "Impact of repetitive manual materials handling and psychosocial work factors on the future prevalence of chronic low-back pain among construction workers," *Scand. J. Work. Environ. Health*, vol. 28, no. 5, pp. 314–323, 2002.

[11] S. M. McGill, “The biomechanics of low back injury: Implications on current practice in industry and the clinic,” *J. Biomech.*, vol. 30, no. 5, pp. 465–475, May 1997, doi: 10.1016/S0021-9290(96)00172-8.

[12] J. Hamill, K. Knutzen, and T. Derrick, *Biomechanical Basis of Human Movement*, 4 edition. Wolters Kluwer Health, 2014.

[13] J. R. Potvin, R. W. Norman, and S. M. McGill, “Reduction in anterior shear forces on the L4L5 disc by the lumbar musculature,” *Clin. Biomech.*, vol. 6, no. 2, pp. 88–96, May 1991, doi: 10.1016/0268-0033(91)90005-B.

[14] M. R. Bracko, “Can We Prevent Back Injuries?,” *ACSMs Health Fit. J.*, vol. 8, no. 4, pp. 5–11, Aug. 2004.

[15] W. S. Marras, S. A. Ferguson, D. Burr, K. G. Davis, and P. Gupta, “Spine loading in patients with low back pain during asymmetric lifting exertions,” *Spine J.*, vol. 4, no. 1, pp. 64–75, Jan. 2004, doi: 10.1016/S1529-9430(03)00424-8.

[16] J. L. Kelsey *et al.*, “An epidemiologic study of lifting and twisting on the job and risk for acute prolapsed lumbar intervertebral disc,” *J. Orthop. Res.*, vol. 2, no. 1, pp. 61–66, 1984, doi: 10.1002/jor.1100020110.

[17] S. Ferguson, W. Marras, and T. Waters, “Quantification of back motion during asymmetric lifting,” *Ergonomics*, vol. 35, pp. 845–59, Jul. 1992, doi: 10.1080/00140139208967366.

[18] H.-K. Kim and Y. Zhang, “Estimation of lumbar spinal loading and trunk muscle forces during asymmetric lifting tasks: application of whole-body musculoskeletal modelling in OpenSim,” *Ergonomics*, vol. 60, no. 4, pp. 563–576, Apr. 2017, doi: 10.1080/00140139.2016.1191679.

[19] H. Schmidt, A. Kettler, F. Heuer, U. Simon, L. Claes, and H.-J. Wilke, “Intradiscal pressure, shear strain, and fiber strain in the intervertebral disc under combined loading,” *Spine*, vol. 32, no. 7, pp. 748–755, Apr. 2007, doi: 10.1097/01.brs.0000259059.90430.c2.

[20] W. Marras and K. Davis, “Spine loading during asymmetric lifting using one versus two hands,” *Ergonomics*, vol. 41, pp. 817–34, Jul. 1998, doi: 10.1080/001401398186667.

[21] D. D. Molinaro, A. S. King, and A. J. Young, “Biomechanical analysis of common solid waste collection throwing techniques using OpenSim and an EMG-assisted solver,” *J. Biomech.*, vol. 104, p. 109704, May 2020, doi: 10.1016/j.jbiomech.2020.109704.

[22] S.-P. Wu, “Psychophysically determined symmetric and asymmetric lifting capacity of Chinese males for one hour’s work shifts,” *Int. J. Ind. Ergon.*, vol. 25, no. 6, pp. 675–682, Jul. 2000, doi: 10.1016/S0169-8141(99)00055-4.

[23] C. Ammendolia, M. S. Kerr, and C. Bombardier, “Back Belt Use for Prevention of Occupational Low Back Pain: A Systematic Review,” *J. Manipulative Physiol. Ther.*, vol. 28, no. 2, pp. 128–134, Feb. 2005, doi: 10.1016/j.jmpt.2005.01.009.

[24] D. Rabinowitz, R. S. Bridger, and M. I. Lambert, “Lifting technique and abdominal belt usage: a biomechanical, physiological and subjective investigation,” *Saf. Sci.*, vol. 28, no. 3, pp. 155–164, Apr. 1998, doi: 10.1016/S0925-7535(97)00080-5.

[25] M. N. M. van Poppel, B. W. Koes, T. van der Ploeg, T. Smid, and L. M. Bouter, “Lumbar Supports and Education for the Prevention of Low Back Pain in Industry: A Randomized Controlled Trial,” *JAMA*, vol. 279, no. 22, pp. 1789–1794, Jun. 1998, doi: 10.1001/jama.279.22.1789.

[26] M. P. de Looze, T. Bosch, F. Krause, K. S. Stadler, and L. W. O’Sullivan, “Exoskeletons for industrial application and their potential effects on physical work load,” *Ergonomics*, vol. 59, no. 5, pp. 671–681, May 2016, doi: 10.1080/00140139.2015.1081988.

[27] A. T. Asbeck, R. J. Dyer, A. F. Larusson, and C. J. Walsh, “Biologically-inspired soft exosuit,” in *2013 IEEE 13th International Conference on Rehabilitation Robotics (ICORR)*, Jun. 2013, pp. 1–8, doi: 10.1109/ICORR.2013.6650455.

[28] P. Dolan and M. A. Adams, “The relationship between EMG activity and extensor moment generation in the erector spinae muscles during bending and lifting activities,” *J. Biomech.*, vol. 26, no. 4–5, pp. 513–522, May 1993, doi: 10.1016/0021-9290(93)90013-5.

[29] M. Abdoli-E, M. J. Agnew, and J. M. Stevenson, “An on-body personal lift augmentation device (PLAD) reduces EMG amplitude of erector spinae during lifting tasks,” *Clin. Biomech.*, vol. 21, no. 5, pp. 456–465, Jun. 2006, doi: 10.1016/j.clinbiomech.2005.12.021.

[30] E. P. Lamers, A. J. Yang, and K. E. Zelik, “Feasibility of a Biomechanically-Assistive Garment to Reduce Low Back Loading During Leaning and Lifting,” *IEEE Trans. Biomed. Eng.*, 2018, doi: 10.1109/TBME.2017.2761455.

[31] M. M. Alemi, J. Geissinger, A. A. Simon, S. E. Chang, and A. T. Asbeck, “A passive exoskeleton reduces peak and mean EMG during symmetric and asymmetric lifting,” *J. Electromyogr. Kinesiol.*, vol. 47, pp. 25–34, Aug. 2019, doi: 10.1016/j.jelekin.2019.05.003.

[32] A. S. Koopman *et al.*, “Biomechanical evaluation of a new passive back support exoskeleton,” *J. Biomech.*, vol. 105, p. 109795, May 2020, doi: 10.1016/j.jbiomech.2020.109795.

[33] S. Toxiri *et al.*, “Back-Support Exoskeletons for Occupational Use: An Overview of Technological Advances and Trends,” *IISE Trans. Occup. Ergon. Hum. Factors*, vol. 7, no. 3–4, pp. 237–249, Oct. 2019, doi: 10.1080/24725838.2019.1626303.

[34] M. Abdoli-E and J. M. Stevenson, “The effect of on-body lift assistive device on the lumbar 3D dynamic moments and EMG during asymmetric freestyle lifting,” *Clin. Biomech.*, vol. 23, no. 3, pp. 372–380, Mar. 2008, doi: 10.1016/j.clinbiomech.2007.10.012.

[35] P. Dolan, M. Earley, and M. A. Adams, “Bending and compressive stresses acting on the lumbar spine during lifting activities,” *J. Biomech.*, vol. 27, no. 10, pp. 1237–1248, Oct. 1994, doi: 10.1016/0021-9290(94)90277-1.

[36] S. Toxiri *et al.*, “Rationale, Implementation and Evaluation of Assistive Strategies for an Active Back-Support Exoskeleton,” *Front. Robot. AI*, vol. 5, 2018, doi: 10.3389/frobt.2018.00053.

[37] B. Chen, L. Grazi, F. Lanotte, N. Vitiello, and S. Crea, “A Real-Time Lift Detection Strategy for a Hip Exoskeleton,” *Front. Neurorobotics*, vol. 12, 2018, doi: 10.3389/fnbot.2018.00017.

[38] T. Zhang and H. Huang, “A Lower-Back Robotic Exoskeleton: Industrial Handling Augmentation Used to Provide Spinal Support,” *IEEE Robot. Autom. Mag.*, vol. 25, no. 2, pp. 95–106, Jun. 2018, doi: 10.1109/MRA.2018.2815083.

[39] X. Yong, Z. Yan, C. Wang, C. Wang, N. Li, and X. Wu, “Ergonomic Mechanical Design and Assessment of a Waist Assist Exoskeleton for Reducing Lumbar Loads During Lifting Task,” *Micromachines*, vol. 10, no. 7, Jul. 2019, doi: 10.3390/mi10070463.

[40] U. Heo, S. J. Kim, and J. Kim, “Backdrivable and Fully-Portable Pneumatic Back Support Exoskeleton for Lifting Assistance,” *IEEE Robot. Autom. Lett.*, vol. 5, no. 2, pp. 2047–2053, Apr. 2020, doi: 10.1109/LRA.2020.2969169.

[41] M. Cempini, S. M. M. De Rossi, T. Lenzi, N. Vitiello, and M. C. Carrozza, “Self-Alignment Mechanisms for Assistive Wearable Robots: A Kinetostatic Compatibility Method,” *IEEE Trans. Robot.*, vol. 29, no. 1, pp. 236–250, Feb. 2013, doi: 10.1109/TRO.2012.2226381.

[42] B. Chen, F. Lanotte, L. Grazi, N. Vitiello, and S. Crea, “Classification of Lifting Techniques for Application of A Robotic Hip Exoskeleton,” *Sensors*, vol. 19, no. 4, Art. no. 4, Jan. 2019, doi: 10.3390/s19040963.

[43] S. Grosu *et al.*, “Driving Robotic Exoskeletons Using Cable-Based Transmissions: A Qualitative Analysis and Overview,” *Appl. Mech. Rev.*, vol. 70, no. 6, Nov. 2018, doi: 10.1115/1.4042399.

[44] A. T. Asbeck, S. M. M. De Rossi, I. Galiana, Y. Ding, and C. J. Walsh, “Stronger, Smarter, Softer: Next-Generation Wearable Robots,” *IEEE Robot. Autom. Mag.*, vol. 21, no. 4, pp. 22–33, Dec. 2014, doi: 10.1109/MRA.2014.2360283.

[45] Y. Mao and S. K. Agrawal, "Design of a Cable-Driven Arm Exoskeleton (CAREX) for Neural Rehabilitation," *IEEE Trans. Robot.*, vol. 28, no. 4, pp. 922–931, Aug. 2012, doi: 10.1109/TRO.2012.2189496.

[46] F. A. Panizzolo *et al.*, "A biologically-inspired multi-joint soft exosuit that can reduce the energy cost of loaded walking," *J. NeuroEngineering Rehabil.*, vol. 13, May 2016, doi: 10.1186/s12984-016-0150-9.

[47] X. Yang *et al.*, "Spine-Inspired Continuum Soft Exoskeleton for Stoop Lifting Assistance," *IEEE Robot. Autom. Lett.*, vol. 4, no. 4, pp. 4547–4554, Oct. 2019, doi: 10.1109/LRA.2019.2935351.

[48] H. K. Ko, S. W. Lee, D. H. Koo, I. Lee, and D. J. Hyun, "Waist-assistive exoskeleton powered by a singular actuation mechanism for prevention of back-injury," *Robot. Auton. Syst.*, vol. 107, pp. 1–9, Sep. 2018, doi: 10.1016/j.robot.2018.05.008.

[49] S. Lee, S. Crea, P. Malcolm, I. Galiana, A. Asbeck, and C. Walsh, "Controlling negative and positive power at the ankle with a soft exosuit," in *2016 IEEE International Conference on Robotics and Automation (ICRA)*, May 2016, pp. 3509–3515, doi: 10.1109/ICRA.2016.7487531.

[50] A. T. Asbeck, R. J. Dyer, A. F. Larusson, and C. J. Walsh, "Biologically-inspired soft exosuit," in *2013 IEEE 13th International Conference on Rehabilitation Robotics (ICORR)*, Jun. 2013, pp. 1–8, doi: 10.1109/ICORR.2013.6650455.

[51] K. A. Witte, A. M. Fatschel, and S. H. Collins, "Design of a lightweight, tethered, torque-controlled knee exoskeleton," in *2017 International Conference on Rehabilitation Robotics (ICORR)*, Jul. 2017, pp. 1646–1653, doi: 10.1109/ICORR.2017.8009484.

[52] S. Toxiri, J. Ortiz, J. Masood, J. Fernández, L. A. Mateos, and D. G. Caldwell, "A wearable device for reducing spinal loads during lifting tasks: Biomechanics and design concepts," in *2015 IEEE International Conference on Robotics and Biomimetics (ROBIO)*, Dec. 2015, pp. 2295–2300, doi: 10.1109/ROBIO.2015.7419116.

[53] M. Abdoli-Eramaki, J. M. Stevenson, S. A. Reid, and T. J. Bryant, "Mathematical and empirical proof of principle for an on-body personal lift augmentation device (PLAD)," *J. Biomech.*, vol. 40, no. 8, pp. 1694–1700, Jan. 2007, doi: 10.1016/j.jbiomech.2006.09.006.

[54] P. Dolan, M. Earley, and M. A. Adams, "Bending and compressive stresses acting on the lumbar spine during lifting activities," *J. Biomech.*, vol. 27, no. 10, pp. 1237–1248, Oct. 1994, doi: 10.1016/0021-9290(94)90277-1.

[55] J. H. van Dieën, P. van der Burg, T. A. Raaijmakers, and H. M. Toussaint, "Effects of repetitive lifting on kinematics: inadequate anticipatory control or adaptive changes?,"

J. Mot. Behav., vol. 30, no. 1, pp. 20–32, Mar. 1998, doi: 10.1080/00222899809601319.

[56] U. Lee, C.-W. Pan, and E. Rouse, "Empirical Characterization of a High-performance Exterior-rotor Type Brushless DC Motor and Drive," Nov. 2019, pp. 8018–8025, doi: 10.1109/IROS40897.2019.8967626.

[57] A. Mazumdar *et al.*, "Synthetic Fiber Capstan Drives for Highly Efficient, Torque Controlled, Robotic Applications," *IEEE Robot. Autom. Lett.*, vol. 2, no. 2, pp. 554–561, Apr. 2017, doi: 10.1109/LRA.2016.2646259.

[58] "Planetary gear ratio calculations." https://woodgears.ca/gear/planetary.html (accessed Nov. 12, 2020).

[59] R. Budynas and K. Nisbett, *Shigley's Mechanical Engineering Design*, 10th edition. New York, NY: McGraw-Hill Education, 2014.

[60] "National Health Statistics Reports, Number 122, December 20, 2018," no. 122, p. 16, 2018.

[61] S. L. Delp *et al.*, "OpenSim: Open-Source Software to Create and Analyze Dynamic Simulations of Movement," *IEEE Trans. Biomed. Eng.*, vol. 54, no. 11, pp. 1940–1950, Nov. 2007, doi: 10.1109/TBME.2007.901024.

[62] A. Seth *et al.*, "OpenSim: Simulating musculoskeletal dynamics and neuromuscular control to study human and animal movement," *PLOS Comput. Biol.*, vol. 14, no. 7, p. e1006223, Jul. 2018, doi: 10.1371/journal.pcbi.1006223.

[63] E. Beaucage-Gauvreau *et al.*, "Validation of an OpenSim full-body model with detailed lumbar spine for estimating lower lumbar spine loads during symmetric and asymmetric lifting tasks," *Comput. Methods Biomech. Biomed. Engin.*, vol. 22, no. 5, pp. 451–464, Apr. 2019, doi: 10.1080/10255842.2018.1564819.

[64] D. Stegeman and H. Hermens, "Standards for suface electromyography: The European project Surface EMG for non-invasive assessment of muscles (SENIAM)," vol. 1, Jan. 2007.

[65] M. A. Sherman, A. Seth, and S. L. Delp, "WHAT IS A MOMENT ARM? CALCULATING MUSCLE EFFECTIVENESS IN BIOMECHANICAL MODELS USING GENERALIZED COORDINATES," *Proc. ASME Des. Eng. Tech. Conf. ASME Des. Eng. Tech. Conf.*, vol. 2013, Aug. 2013, doi: 10.1115/DETC2013-13633.

[66] G. Borg, *Borg's perceived exertion and pain scales*. Champaign, IL, US: Human Kinetics, 1998, pp. viii, 104.

[67] S. Park and W. Yoo, "Comparison of exercises inducing maximum voluntary isometric contraction for the latissimus dorsi using surface electromyography," *J.*

Electromyogr. Kinesiol., vol. 23, no. 5, pp. 1106–1110, Oct. 2013, doi: 10.1016/j.jelekin.2013.05.003.

[68] F. J. Vera-Garcia, J. M. Moreside, and S. M. McGill, "MVC techniques to normalize trunk muscle EMG in healthy women," *J. Electromyogr. Kinesiol.*, vol. 20, no. 1, pp. 10–16, Feb. 2010, doi: 10.1016/j.jelekin.2009.03.010.

[69] J. K.-F. Ng, V. Kippers, M. Parnianpour, and C. A. Richardson, "EMG activity normalization for trunk muscles in subjects with and without back pain," *Med. Sci. Sports Exerc.*, vol. 34, no. 7, pp. 1082–1086, Jul. 2002, doi: 10.1097/00005768-200207000-00005.

[70] M. Christophy, N. A. Faruk Senan, J. C. Lotz, and O. M. O'Reilly, "A Musculoskeletal model for the lumbar spine," *Biomech. Model. Mechanobiol.*, vol. 11, no. 1, pp. 19–34, Jan. 2012, doi: 10.1007/s10237-011-0290-6.

[71] C. Pizzolato *et al.*, "CEINMS: A toolbox to investigate the influence of different neural control solutions on the prediction of muscle excitation and joint moments during dynamic motor tasks," *J. Biomech.*, vol. 48, no. 14, pp. 3929–3936, Nov. 2015, doi: 10.1016/j.jbiomech.2015.09.021.

[72] M. B. Yandell, D. M. Ziemnicki, K. A. McDonald, and K. E. Zelik, "Characterizing the comfort limits of forces applied to the shoulders, thigh and shank to inform exosuit design," *PLOS ONE*, vol. 15, no. 2, p. e0228536, Feb. 2020, doi: 10.1371/journal.pone.0228536.

[73] R. Norman, R. Wells, P. Neumann, J. Frank, H. Shannon, and M. Kerr, "A comparison of peak vs cumulative physical work exposure risk factors for the reporting of low back pain in the automotive industry," *Clin. Biomech.*, vol. 13, no. 8, pp. 561–573, Dec. 1998, doi: 10.1016/S0268-0033(98)00020-5.